

# A Doubly Robust Machine Learning Approach for Disentangling Treatment Effect Heterogeneity with Functional Outcomes

Filippo Salmaso<sup>1,2\*</sup>, Lorenzo Testa<sup>1,3\*</sup>, and Francesca Chiaromonte<sup>1,4#</sup>

<sup>1</sup>L'EMbeDS, Sant'Anna School of Advanced Studies, Pisa, Italy

<sup>2</sup>School of Pharmaceutical Science, University of Geneva, Genève, Switzerland

<sup>3</sup>Department of Statistics & Data Science, Carnegie Mellon University, Pittsburgh PA, US

<sup>4</sup>Department of Statistics, Penn State University, University Park PA, US

\*These authors contributed equally

#Corresponding author

filippo.salmaso@unige.ch lorenzo@stat.cmu.edu fxc11@psu.edu

February 12, 2026

## Abstract

Causal inference is paramount for understanding the effects of interventions, yet extracting personalized insights from increasingly complex data remains a significant challenge for modern machine learning. This is the case, in particular, when considering functional outcomes observed over a continuous domain (e.g., time, or space). Estimation of heterogeneous treatment effects, known as CATE, has emerged as a crucial tool for personalized decision-making, but existing meta-learning frameworks are largely limited to scalar outcomes, failing to provide satisfying results in scientific applications that leverage the rich, continuous information encoded in functional data. Here, we introduce FOCaL (Functional Outcome Causal Learning), a novel, doubly robust meta-learner specifically engineered to estimate a *functional* heterogeneous treatment effect (F-CATE). FOCaL integrates advanced functional regression techniques for both outcome modeling and functional pseudo-outcome reconstruction, thereby enabling the direct and robust estimation of F-CATE. We provide a rigorous theoretical derivation of FOCaL, demonstrate its performance and robustness compared to existing non-robust functional methods through comprehensive simulation studies, and illustrate its practical utility on diverse real-world functional datasets. FOCaL advances the capabilities of machine intelligence to infer nuanced, individualized causal effects from complex data, paving the way for more precise and trustworthy AI systems in personalized medicine, adaptive policy design, and fundamental scientific discovery.

## 1 Introduction

Causal inference has become a cornerstone of modern statistics and machine learning, providing a formal language and a rigorous toolkit for moving beyond associative relationships to answer substantial questions about the effects of interventions in a variety of fields, including medicine (Prosperi et al., 2020), genomics (Du et al., 2025), economics (Varian, 2016), and the social sciences (Imbens, 2024). Early developments in this field (Rubin, 1974, 2005) established the so-called *counterfactual* framework for estimating the *Average Treatment Effect* (ATE), which measures the mean effect of a treatment across an entire population.

Although the ATE is a valuable summary estimand, it often masks significant underlying variation. In many real-world scenarios, the effect of a treatment is not uniform but varies across individuals with different characteristics. For example, a new drug may be highly effective for one patient subgroup but have little to no effect on another. This phenomenon, known as *treatment effect heterogeneity*, has become a critical

frontier in causal inference. Understanding “what works for whom” is essential, e.g., for personalized medicine and targeted policy implementation (Xu et al., 2024). The central statistical target for quantifying this heterogeneity is the *Conditional Average Treatment Effect* (CATE), which measures the average treatment effect for subpopulations defined by a specific set of covariates. Estimating the CATE allows one to map how the treatment effect changes across the covariate space.

The challenge of estimating the CATE has been tackled through the development of effective and flexible machine learning methods known as *meta-learners* (Caron et al., 2022; Molak, 2023; Wager, 2024). These algorithms leverage the predictive power of modern machine learning, typically by reframing the causal question as a sequence of supervised learning problems. Using non-parametric models such as random forests, gradient boosting, or neural networks one can capture complex relationships in the data without imposing strong parametric assumptions on the CATE structure. Thus, machine learning techniques – including black-boxes – can facilitate inference on nuanced causal effects.

Concurrently, the nature of the data being collected in many scientific fields has evolved in complexity, presenting compelling new frontiers for machine intelligence. In particular, advances in technology have led to an explosion of *functional data*, where each observation is not a single number or a vector, but an entire function recorded over a continuum like time or space (Kokoszka and Reimherr, 2017; Ramsay and Silverman, 2005). Examples include longitudinal studies where medical or wearable devices are used to record patients’ biometrics over time (Boschi et al., 2024a; Jeong et al., 2024), epidemiological studies where infectious diseases are tracked across spatiotemporal domains (Boschi et al., 2021, 2026), neuroscience studies where activity is monitored over time and across the volume of the brain (Boschi et al., 2024d; Qi and Luo, 2018), and economic and financial studies where metrics of interest are measured over time (Caldeira and Torrent, 2017; Cremona et al., 2023; Esposito et al., 2022). This type of data poses unique challenges and offers unique opportunities for robust and adaptive machine learning approaches. *Functional Data Analysis* (FDA) provides a set of tools to analyze such data, properly accounting for the inherent smoothness and structure of curves and surfaces, and avoiding the pitfalls of treating them as simple high-dimensional vectors – a crucial step for developing intelligent systems that can truly understand and reason about complex, continuous processes.

Our work sits at the intersection of causal inference and FDA; while both these areas of statistics are quite advanced and rapidly evolving, machine learning methods to address causal questions within the context of functional data remain underdeveloped. A significant gap exists in the literature for methods to estimate heterogeneous treatment effects with functional outcomes, and this gap hinders the development of truly personalized and adaptive AI solutions. Traditional meta-learner methods for estimating heterogeneous treatment effects cannot be applied directly, and current functional data techniques are either designed for settings without access to additional covariates (Cremona et al., 2018), or model outcomes with non-robust tools such as function-on-scalar regression (Ecker et al., 2024; Ieva et al., 2025) which may perform poorly if the model is misspecified, limiting their utility in real-world applications. Relevant exceptions, limited to the estimation of average treatment effects, include Liu et al. (2024); Raykov et al. (2025); Testa et al. (2025), who provide estimators that are robust to some forms of model misspecification. This work aims to bridge the gap by introducing a novel meta-learner that leverages advanced machine learning techniques for F-CATE estimation; that is, estimation of the CATE in settings with functional outcome and scalar predictors.

Our meta-learner, which we call FOCaL (Functional Outcome Causal Learning), enjoys double robustness and significantly advances the capabilities of machine intelligence in these complex settings. We provide a careful derivation of FOCaL, describe its statistical properties, and demonstrate its practical advantages through a comprehensive simulation study. We also showcase its practical utility through the analysis of two datasets: the SHARE dataset (Alcser et al., 2005), where we study the heterogeneous effects of chronic conditions on the time progression of quality of life indicators, and a dataset on the COVID-19 epidemic in Italy (Boschi et al., 2026), where we investigate the causal implications of distributed primary health care on COVID-19 mortality patterns.

This work provides a rigorous foundation for applying modern causal learning techniques to the rich data structures increasingly encountered in scientific research, paving the way for more sophisticated and

trustworthy AI systems capable of deep causal understanding and precision decision-making.

## 2 Results

### 2.1 Overview of FOCaL

Building upon the principles of doubly robust meta-learning (Kennedy, 2023), FOCaL estimates (and quantifies the uncertainty behind) the causal effect of a binary treatment on a functional outcome, controlling for (i.e., conditioning on) measured categorical and scalar confounders, and thus capturing heterogeneity in causal effects. FOCaL requires some standard causal inference assumptions, including conditional ignorability and positivity (Tsiatis, 2006), and operates on a collection of  $n$  i.i.d. samples  $\mathcal{D}_i = (X_i, A_i, \mathcal{Y}_i)$ ,  $i = 1, \dots, n$ , where  $X_i$  is a set of pretreatment scalar and/or categorical covariates,  $A_i$  is a binary variable indicating whether observation  $i$  has been exposed to a treatment ( $A_i = 1$ ) or not ( $A_i = 0$ ), and  $\mathcal{Y}_i$  is a functional outcome measured over a continuous domain. Our approach can be applied regardless of the dimension of this domain, but for simplicity we will consider a one-dimensional domain such as time – so we can think of  $\mathcal{Y}_i$  as a smooth curve satisfying standard FDA assumptions (Kokoszka and Reimherr, 2017). Based on the available samples, FOCaL returns an estimate of  $\theta^*(x)$ , the functional conditional average treatment effect (F-CATE). For each specification  $x$  of the covariates, the F-CATE is itself a function unfolding on the same domain as the outcomes  $\mathcal{Y}_i$ 's; its dependence on  $x$  captures heterogeneity in the response to treatment between individuals with different characteristics (formal definitions, along with more detail on assumptions and theoretical derivations, are provided in the Methods).

FOCaL's core pipeline consists of three interconnected stages (see Figure 1). In the first, FOCaL leverages flexible machine learning algorithms to estimate from the data some crucial, so-called *nuisance* functions (Tsiatis, 2006): the *regression functions*  $\mu^{*(a)}(x)$ ,  $a \in \{0, 1\}$ , which represent the expected functional outcome given the covariates and the treatment assignment, and the *propensity score*  $\pi^*(x)$ , which represents the probability of receiving the treatment given the covariates. The estimates  $\hat{\mu}^{(a)}(x)$ ,  $a \in \{0, 1\}$  are obtained with advanced functional regression techniques (Boschi et al., 2024c,d; Yao et al., 2021), where the covariates map into an entire functional response over the continuous domain under consideration, allowing FOCaL to learn the expected shape and trajectory of the outcome. The estimate  $\hat{\pi}(x)$  is typically handled as a standard binary classification problem; a number of powerful classifiers can be employed to yield an estimate of  $\Pr[A = 1 | X = x]$ . The use of flexible, data-driven machine learning models in these initial estimations is fundamental, as it allows FOCaL to accurately capture complex, non-linear relationships without imposing rigid parametric assumptions, and integrating information coming from different data modalities (scalar and categorical covariates).

In the second stage, FOCaL reconstructs two functional pseudo-outcomes,  $\gamma^{*(a)}(\mathcal{D}_i)$ ,  $a \in \{0, 1\}$ , for each individual  $i = 1, \dots, n$ . These pseudo-outcomes are specifically defined to isolate the causal effect of the treatment on the functional outcome, adjusting for potential confounding. They are estimated as:

$$\hat{\gamma}^{(1)}(\mathcal{D}_i) = \hat{\mu}^{(1)}(X_i) + \frac{A_i}{\hat{\pi}(X_i)} (\mathcal{Y}_i - \hat{\mu}^{(1)}(X_i)), \quad \hat{\gamma}^{(0)}(\mathcal{D}_i) = \hat{\mu}^{(0)}(X_i) + \frac{1 - A_i}{1 - \hat{\pi}(X_i)} (\mathcal{Y}_i - \hat{\mu}^{(0)}(X_i)). \quad (1)$$

This formulation endows FOCaL with its crucial *doubly robust* property: the estimators for the functional pseudo-outcomes remain asymptotically consistent even if either the functional outcome modeling that produces  $\hat{\mu}^{(a)}(x)$ ,  $a \in \{0, 1\}$ , or the propensity score modeling that produces  $\hat{\pi}(x)$  are misspecified, provided one of the two is correctly specified. This inherent robustness is a significant advantage for machine intelligence systems deployed in real-world scenarios, where achieving perfect model specification is often impractical. In particular, in the context of our proposal, double robustness enhances the reliability of causal inferences drawn from functional data.

In the third stage, FOCaL estimates the F-CATE  $\theta^*(x)$ . This is accomplished by performing a final regression of the difference in the computed functional pseudo-outcomes  $\hat{\gamma}^{(1)}(\mathcal{D}) - \hat{\gamma}^{(0)}(\mathcal{D})$  on the covariates. This step utilizes again advanced functional regression techniques to model how the entire functional treatment effect changes across the covariate space. The output is a function  $\hat{\theta}(x)$  that, for any given covariate profile  $x$ , describes the expected difference in the functional outcome due to treatment and quantifies its uncertainty

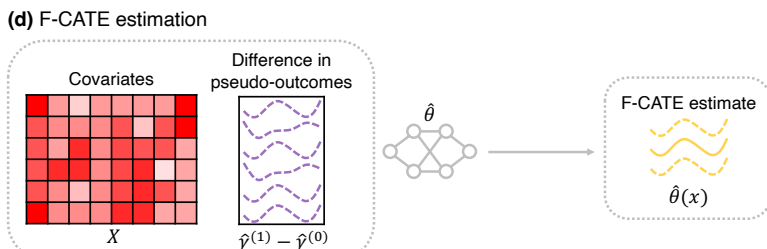
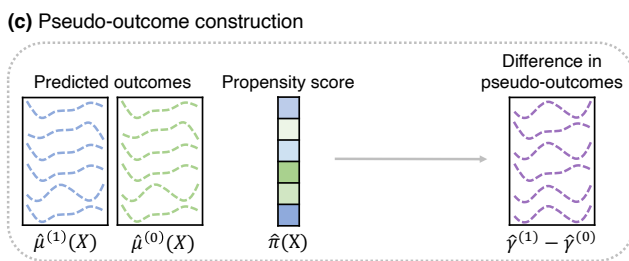
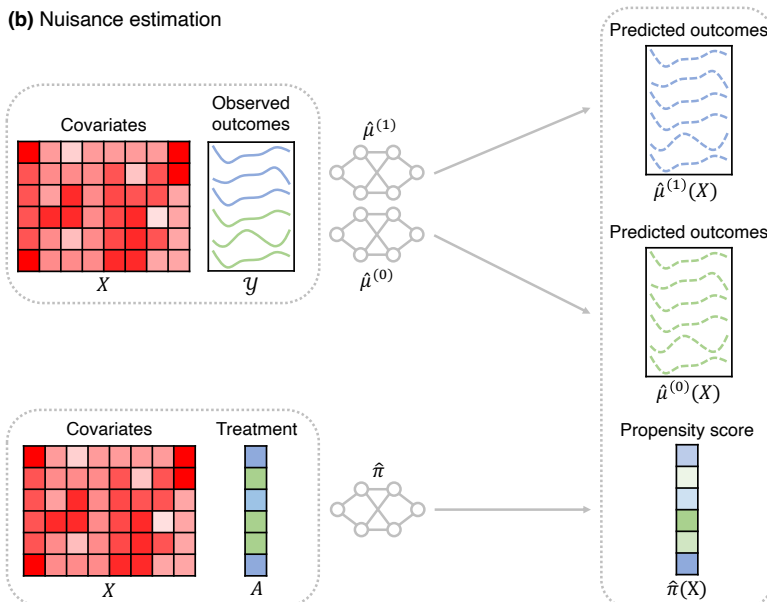
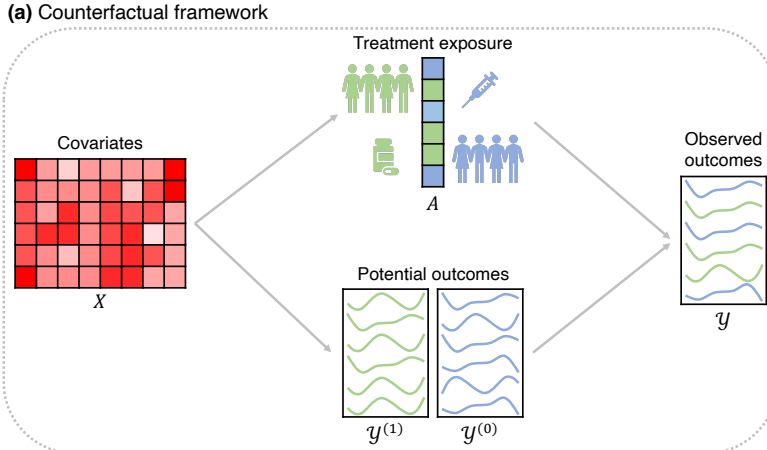


**Figure 1: An overview of FOCaL.**

**(a)** The counterfactual framework. For every subject defined by the covariates in  $X$ , two potential functional outcomes exist:  $\mathcal{Y}^{(1)}$  (outcome under treatment) and  $\mathcal{Y}^{(0)}$  (outcome under control). The treatment assignment  $A$  acts as a selector, determining which of these potential trajectories is realized as the observed outcome  $\mathcal{Y}$ , leaving the other unobserved (counterfactual). **(b)** Nuisance function estimation (FOCaL stage 1). Flexible machine learning models are employed to estimate the conditional outcome regressions  $\hat{\mu}^{(a)}(X)$  for the two treatment arms  $a = 0, 1$ , and the propensity score  $\hat{\pi}(X)$ . **(c)** Pseudo-outcome construction (FOCaL stage 2). The nuisance estimates are combined to reconstruct functional pseudo-outcomes using a doubly robust formulation, isolating the difference  $\hat{\gamma}^{(1)} - \hat{\gamma}^{(0)}$  adjusted for confounding. **(d)** F-CATE estimation and inference (FOCaL stage 3). The difference in pseudo-outcomes is regressed on the covariates to yield the final estimator  $\hat{\theta}(x)$ , which quantifies the heterogeneous functional treatment effect across the covariate space. Dashed lines represent simultaneous confidence bands computed around the estimated F-CATE to capture uncertainty.

by providing a *simultaneous confidence band* which contains the true  $\theta^*(x)$  with at least a user-specified probability. Through this process, FOCaL moves beyond scalar averages, providing granular, reliable, and interpretable causal insights that pinpoint not only who benefits from an intervention, but precisely how their functional response (e.g., the evolution of a quality of life indicator, the progression of mortality during an epidemic) is expected to change. FOCaL thus empowers machine intelligence to reason effectively about interventions in complex, dynamic systems.

## 2.2 Simulation results provide strong evidence of FOCaL’s effectiveness

To rigorously evaluate FOCaL’s ability to recover heterogeneous functional treatment effects, we conduct a comprehensive simulation study designed to mimic challenging real-world conditions. We generate datasets of  $n = 5000$  observations with time-varying functional outcomes defined as linear functions of coefficients with a Matérn covariance structure that induces realistic smoothness and correlation. Crucially, the data generating process features non-linear confounding between covariates and treatment assignment, creating a setting where simple linear adjustments would fail. We test the estimator across four distinct scenarios – ranging from fully accurate model specification to simultaneous misspecification of both the propensity score and outcome regression components. These scenarios are created introducing non-linear transformations of the covariates into the nuisance models.

Our analysis first highlights the significant risks of relying on standard observational metrics in such complex settings. As visualized in Figure 2a, naive comparisons of the observed mean trajectories between treated and untreated populations exhibit substantial bias, failing to account for the underlying confounding structure (due to covariate imbalance, see Figure 2b). In contrast, FOCaL effectively corrects for these biases. Even when nuisance models are imperfect, FOCaL reconstructs the counterfactual trajectories with high fidelity, realigning the estimated effects, obtained by averaging the difference in pseudo-outcomes computed through FOCaL’s second stage, with the ground truth and demonstrating the necessity of robust causal adjustments over simple associative comparisons (Figure 2c).

The primary strength of FOCaL – its double robustness – is confirmed by the stability of its estimation accuracy under stress. We quantify performance using the Aggregated Root Mean Squared Error (ARMSE, see Methods for a definition) between the estimated and true Functional Conditional Average Treatment Effects (F-CATE). FOCaL exhibits negligible performance deterioration when either the propensity score or the outcome regression is misspecified, effectively matching the accuracy achieved under full model specification. As shown in the ARMSE boxplots (Figure 2e), significant error inflation and variance degradation emerge only in the “worst-case” scenario where both nuisance models are simultaneously misspecified.

Furthermore, FOCaL successfully recovers the granular structure of treatment effect heterogeneity. The estimated F-CATE surfaces (Figure 2d) accurately map how the treatment effect varies continuously across both the functional domain and the covariate space, capturing the non-linear interactions driven by the data generating process. These findings empirically corroborate the theoretical guarantees of our framework, suggesting that FOCaL can provide reliable, nuanced causal insights in scientific applications where the true data-generating mechanisms are often complex and rarely known with certainty.

## 2.3 FOCaL reveals the heterogeneous effects of chronic conditions on quality of life

To demonstrate the use of FOCaL, we apply it to data from SHARE (*Survey of Health, Aging and Retirement in Europe*), a large longitudinal study comprising thousands of subjects followed through eight data collection surveys (called “waves”) conducted between 2004 and 2020 (Alcser et al., 2005; Bergmann et al., 2017; Börsch-Supan, 2020; Börsch-Supan et al., 2013).

Specifically, we employ FOCaL to investigate the heterogeneous causal effects of chronic conditions on longitudinal indicators of quality of life in different subpopulations. To ensure reliable curve estimation, we focus on 1518 subjects who participated in at least seven (out of eight) waves (see Methods for full detail on data preprocessing). For each subject, we consider two functional indicators of quality of life – a mobility

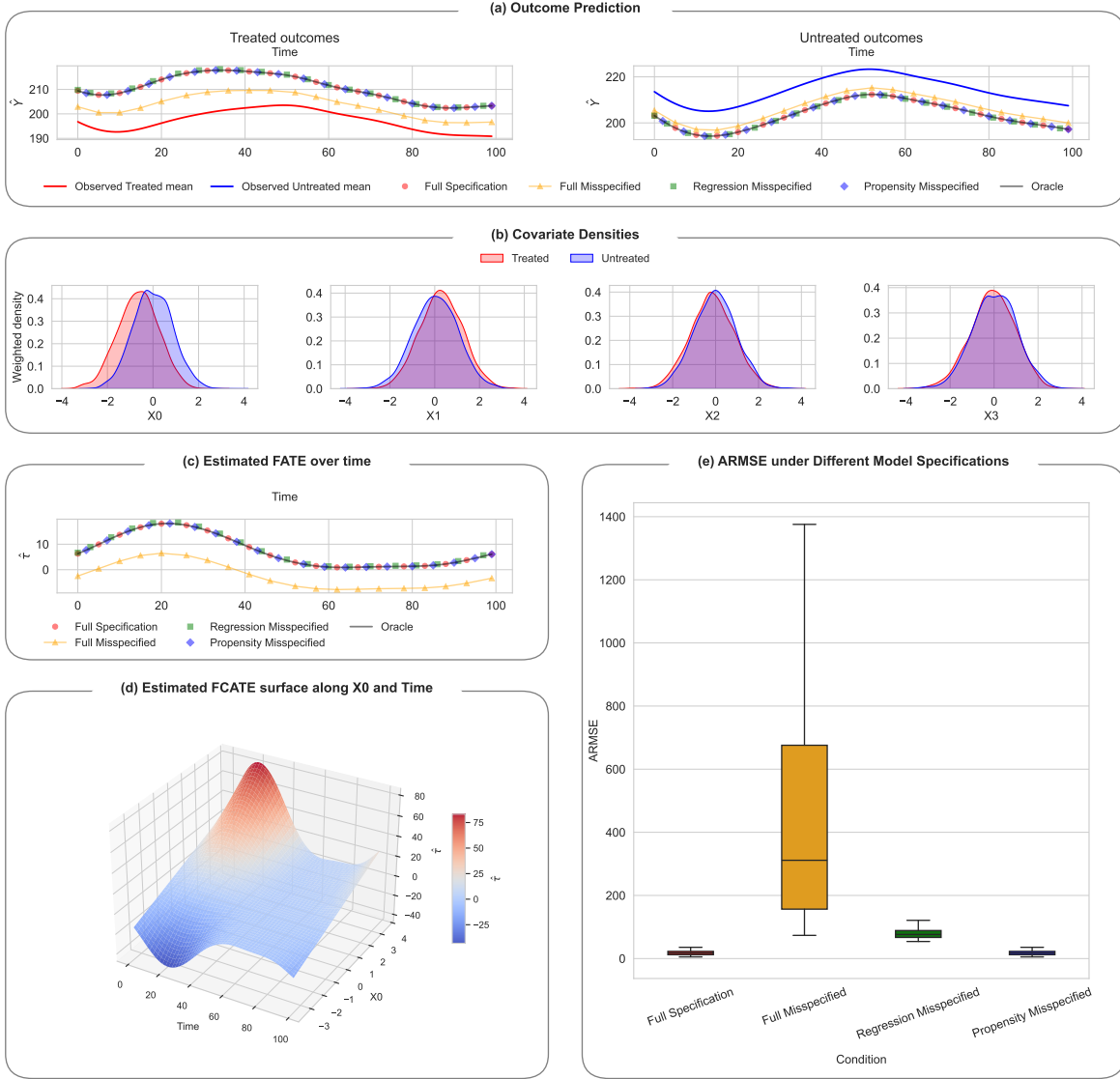


**Figure 2:** Performance and robustness of FOCaL in simulated settings. **(a)** Comparison of functional outcome trajectories for treated (left) and untreated (right) populations. Solid lines represent the naive observed means, which exhibit significant bias due to confounding (departures from the Oracle, which is shown in solid gray). Lines with symbols (circle, triangle, squares, diamonds) represent the model-recovered trajectories under different specifications; note that FOCaL accurately reconstructs the true curves even when one nuisance component is misspecified, correcting the bias inherent in the raw data. **(b)** Density plots for original covariates ( $X_j$ ,  $j = 0, 1, 2, 3$ ) illustrating the distributional imbalance between treated (red) and control (blue) groups, which motivates the adjustment (the distributions differ especially for  $X_0$ ). **(c)** Evaluation of FATE estimation accuracy. The line plot displays the estimated Functional Average Treatment Effect (FATE) over time; estimates remain stable and close to the truth (Oracle, in solid grey) unless both models are misspecified. **(d)** Example of F-CATE target. The surface plot visualizes the estimated Functional Conditional Average Treatment Effect (F-CATE) as a function of time and covariate  $X_0$ , demonstrating FOCaL's ability to capture complex, heterogeneous effect surfaces (the true surface is shown for reference in Supplementary Figure C.1). **(e)** Evaluation of F-CATE estimation accuracy. The boxplots show Aggregated Root Mean Squared Error (ARMSE) values across 1000 Monte Carlo replications, confirming that sizeable error inflation occurs only under double misspecification.

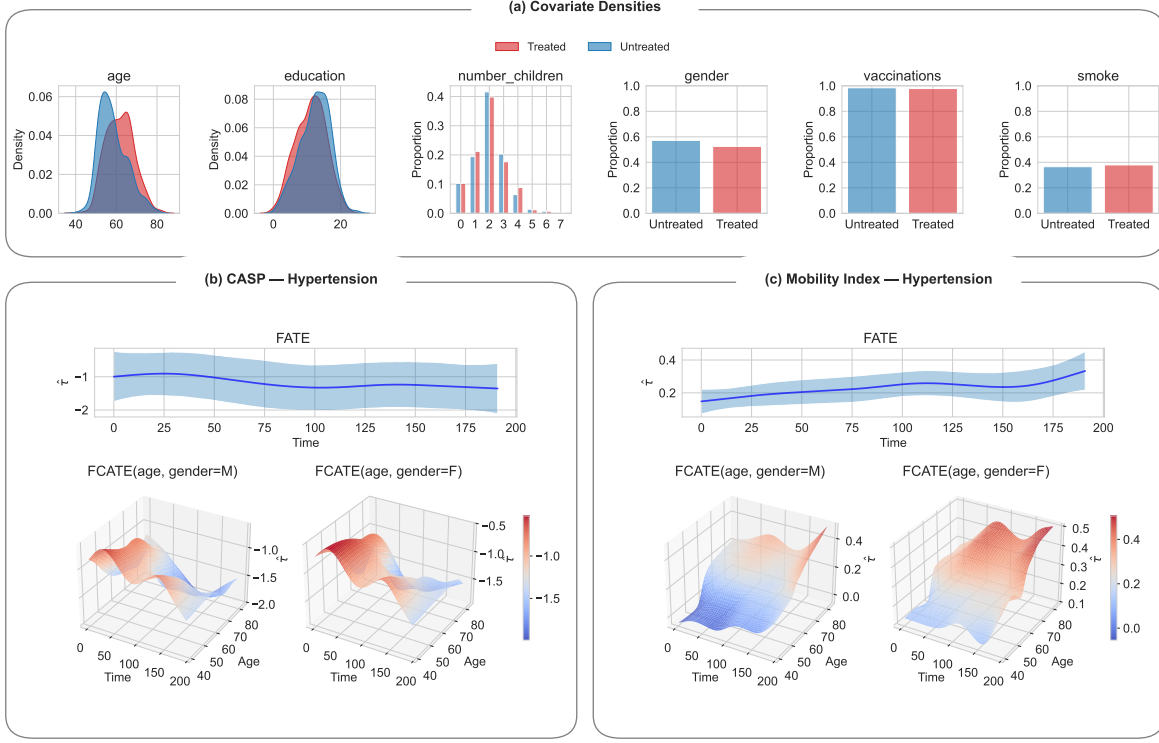


**Figure 3:** Heterogeneous impact of hypertension on quality of life trajectories (SHARE study). **(a)** Distributions of key baseline covariates for treated (hypertension) and control populations. While most socio-demographic factors show comparable spread, age exhibits a sizeable imbalance between groups; this motivates the propensity adjustment performed by FOCaL. **(b)** Results for CASP. The estimated Functional Average Treatment Effect (FATE) and the associated simultaneous 95% confidence band over the 192-month observation window indicate a statistically significant decline in well-being: hypertension exerts a negative and progressively larger effect on the CASP quality of life score. The estimated F-CATE surfaces characterizing the heterogeneity of the causal effect conditioned on age and gender (all other binary and scalar covariates are set to their modal and mean values, respectively) show that the detrimental effect of hypertension intensifies with age across the entire time domain. Gender plays an intercept-like role, amplifying the absolute magnitude of the functional effect for males without markedly altering the shape of the surface. **(c)** Results for Mobility Index. The estimated Functional Average Treatment Effect (FATE) and the associated simultaneous 95% confidence band show a positive, increasing, and statistically significant effect on the Mobility Index (higher values indicate greater impairment). The estimated F-CATE surfaces reveal a distinct temporal profile for older individuals – a moderate mid-period exacerbation followed by a sharp, late-stage increase during the final stages of the time domain. This profile is more pronounced and occurs earlier for women than for men. Note: the plots for CASP and the Mobility Index have response-specific vertical scales (the two outcomes are measured on different scales; see Supplementary Figure D.4).

index and the Quality of Life Scale (CASP) (Hyde et al., 2003) measured over 192 months; binary status relative to the chronic disease hypertension; and a variety of socio-demographic and healthcare related covariates (see Table D.1 in the Supplementary Information).

Following the logic of the counterfactual model, we define the causal effect of a chronic disease on a quality of life indicator as the expected difference between the functional outcome if a subject had, or did not have, the chronic disease. Therefore, we form treatment groups identifying subjects who present chronic conditions at the beginning of the study, and control groups identifying subjects who never develop chronic conditions throughout the study period. This results in 419 treated subjects and 577 control subjects for hypertension.

For each functional outcome, we then fit FOCaL using a function-on-scalar neural network specification for the regression function  $\hat{\mu}^{(a)}$ , and logistic regression for the propensity score  $\hat{\pi}^{(a)}$ . No time-varying or post-baseline variables beyond the cohort definition are used in the propensity score or outcome models. Results are shown in Figure 3. In the aggregate, the estimated Functional Average Treatment Effects (FATE), obtained by averaging the difference in pseudo-outcomes computed through FOCaL’s second stage, reveal a coherent and clinically consistent narrative regarding the impact of hypertension on quality of life. We observe a progressive deterioration in well-being for treated subjects across both functional outcomes. Specifically, hypertension causes a deepening negative effect on the CASP score over time. Simultaneously, it leads to an increasing positive effect on the mobility index; since higher mobility scores indicate greater physical impairment, this confirms that the condition exerts a detrimental force on both psychological and physical dimensions of health.

Next, to move beyond aggregate summaries and uncover the drivers of this variation, we turn to a more refined analysis using F-CATE estimates. Specifically, we examine the estimated F-CATE surfaces conditioned on age and gender, as these variables represent critical axes of interest from both scientific and policy perspectives. Moreover, as shown by the distributions in Figure 3a, age exhibits the strongest imbalance between treated and control groups, underscoring the importance of the proper correction performed by FOCaL. The detrimental impact of age on CASP can be observed across the entire temporal domain and intensifies markedly with age, as reported by [Anderson \(1999\)](#); [Lloyd-Jones et al. \(2005\)](#). Specifically, the negative effect is relatively stable across the 192-month observation window for younger individuals, and sharpens over time for older individuals, suggesting a decreased resilience for the latter. Furthermore, gender appears to play an “intercept” role – amplifying the absolute magnitude of the effect of hypertension for male subjects, a result supported by previous clinical evidence ([Cutler et al., 2008](#); [Everett and Zajacova, 2015](#); [Hayes and Taler, 1998](#); [Sandberg and Ji, 2012](#); [Vitale et al., 2010](#)). Concerning the mobility index, the estimated F-CATE surface reveals a distinct temporal profile for older individuals, characterized by a moderate mid-period exacerbation followed by a sharp, late-stage increase (a “bump” in the estimated surface) during the final stages of the analysis. These observations align with previous literature ([Burt et al., 1995](#); [Ostchega et al., 2007](#)). Notably, the role of gender in this context is to anticipate and exacerbate the profile for women; older women appear to experience the adverse consequences of hypertension on mobility earlier and more severely than older men ([Alqahtani and Alenazi, 2025](#)).

## 2.4 FOCaL sheds light on the heterogeneous role of distributed primary health care in shaping COVID-19 mortality patterns

To further demonstrate the practical value of FOCaL, we use it to investigate the heterogeneous causal effects of distributed primary health care on COVID-19 mortality patterns during the first two pre-vaccine epidemic waves in Italy ([Boschi et al., 2021, 2026](#)). This application showcases FOCaL’s capability to handle complex spatiotemporal domains where mortality patterns are expressed as functional outcomes.

The data encompasses all 107 Italian provinces throughout the two major pre-vaccine waves of the pandemic. We use as observation windows the 150 days from February 25, 2020 to July 23, 2020 for the first wave, and the 150 days from October 1, 2020 to February 27, 2021 for the second. The first wave was characterized by dramatic, spatially concentrated mortality peaks, particularly in northern regions like Lombardia. In contrast, the second wave was less dramatic, more widespread and asynchronous across the country. The main goal of this analysis is to evaluate the heterogeneous causal effects of distributed primary health care on province-level COVID-19 mortality rate trajectories. We define the treatment using records of the number of adults per family doctor (see Methods for details); “treated” provinces are those with higher ratios, i.e. fewer family doctors, and thus poorer distributed primary health care.

The analysis incorporates several critical socio-demographic and environmental covariates that may confound the relationship between mortality and the treatment, including the percentage of the population over 65 years of age; average beds per hospital, students per classroom and employee per firm (proxies for the ability of hospitals, schools and workplaces to act as contagion hubs), and PM10 pollution levels. In addition, following the logic of [Boschi et al. \(2026\)](#), we consider the covariate “area before” – a province-specific standardized metric evaluating the area under the mortality curve up to the point when restriction measures

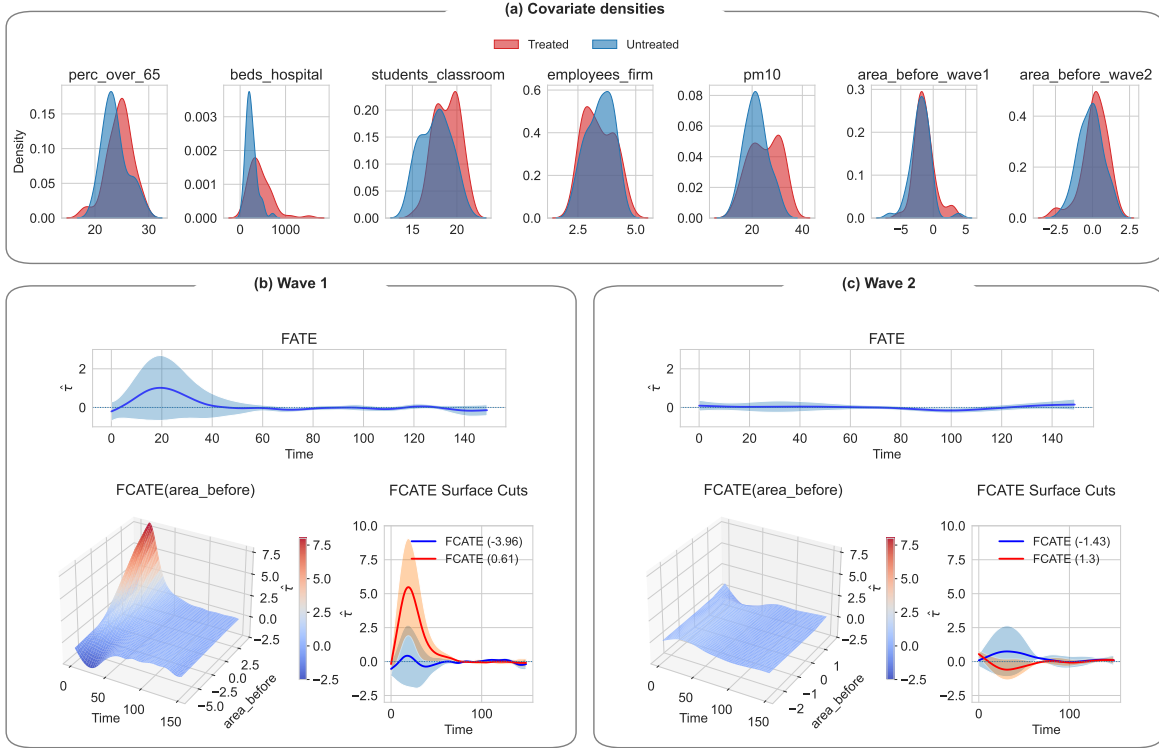


**Figure 4:** Heterogeneous impact of availability of primary health care on COVID-19 mortality patterns (COVID-19 study). **(a)** Distribution of key socio-demographic and environmental baseline covariates for provinces with high (“Treated”) versus low (“Untreated”) number of adults per primary care physician (treated provinces are those with poorer distributed primary health care). Sizeable imbalances between groups are observed in most of the covariates, motivating the propensity adjustment performed by FOCaL. **(b)** Wave 1 results. Top: The estimated Functional Average Treatment Effect (FATE) for the first wave (February-July 2020) suggests that poor distributed primary health care exacerbated mortality in the initial stages, but this is non-significant based on the 95% confidence band. Bottom left: The estimated F-CATE surface conditioned on the “area before” standardized metric disaggregates this effect, revealing a dramatic escalation in provinces with the highest early outbreak intensity, and thus pinpointing how poor distributed primary health care was most consequential where the epidemic had the strongest early momentum. Bottom right: Cuts of the surface plot at the 10<sup>th</sup> (blue) and 90<sup>th</sup> (red) percentiles of the marginal distribution of “area before”, with 90% confidence bands supporting strong significance at the latter. **(c)** Wave 2 results. Top: The estimated FATE for the second wave (October 2020–February 2021) appears rather flat with a tight 95% confidence band around 0, suggesting a negligible impact of distributed primary health care during the more widespread and asynchronous epidemic unfolding that characterized this wave compared to the first. Bottom left: The estimated F-CATE surface confirms a negligible impact also when conditioning on “area before”. Bottom right: Cuts of the surface plot at the 10<sup>th</sup> (blue) and 90<sup>th</sup> (red) percentiles of the marginal distribution of “area before”, again with 90% bands.

were imposed nationally or locally. This standardized cumulative mortality captures the degree to which the epidemic was able to “build up” within a province prior to the implementation of lockdowns and social distancing – avoiding the use of case counts, which were highly unreliable. As shown in Figure 4a, several of the covariates under consideration exhibit marked imbalances between “treated” and “untreated” provinces, thus necessitating the adjustment provided by FOCaL.

The estimated Functional Average Treatment Effects (FATE), obtained by averaging the difference in pseudo-outcomes computed through FOCaL’s second stage, fail to provide a meaningful picture of the impacts of distributed primary health care on mortality. In fact, in both the first and second wave (Figure 4b and c,

top), the estimated FATE trajectories are not statistically significant. Thus, marginal averages lead to the conclusion that the availability of family doctors did not have a role in curbing mortality.

However, this lack of statistical significance masks heterogeneous causal impacts. To disaggregate such impacts, we turn to the F-CATE surfaces conditioning on “area before” – a standardized metric of early epidemic momentum. By focusing specifically on the interaction between “area before” and the temporal progression of mortality, FOCaL reveals a striking and localized story. During the first wave, the estimated F-CATE surface (Figure 4b, bottom) shows a dramatic and significant peak in the treatment effect for provinces with high early epidemic momentum. This pinpoints poor distributed primary health care as a primary driver of mortality exactly in those provinces where COVID-19 had established a strong foothold before the lockdowns. In these provinces, family doctors made a decisive difference as the critical first line of defense, particularly at a stage when standardized clinical protocols and dedicated assistance infrastructures were not yet in place. In contrast, the estimated F-CATE surface for the second wave (Figure 4c, bottom), in agreement with the aggregate effect, reflects a weakening and flattening of these dynamics. The relative importance of primary care in curbing mortality diminished as the epidemic became more geographically widespread and asynchronous, and as the broader healthcare system integrated more mature and diverse response mechanisms. These findings illustrate FOCaL’s ability to provide granular, spatiotemporal insights – unveiling how local conditions and the timing of the outbreak modulated the role of distributed primary health care.

### 3 Discussion

In this paper, we introduce FOCaL (Functional Outcome Causal Learning), a novel doubly robust meta-learner designed to estimate heterogeneous, covariate-dependent treatment effects when outcomes are expressed as functions over a continuous domain. Our proposal addresses a critical gap in the causal inference literature, where existing meta-learning approaches are largely confined to scalar outcomes, thereby failing to fully leverage the rich, continuous information inherent in functional data. By integrating advanced machine learning and functional data analysis tools, FOCaL advances the capabilities of machine intelligence to provide nuanced and individualized causal insights.

A key strength of FOCaL lies in its *doubly robust* design, a property inherited and extended from the well-established DR-Learner framework (Kennedy, 2023). This ensures that FOCaL estimates of the F-CATE remain asymptotically consistent even if one of the models employed for the nuisance functions (functional outcome regressions and propensity score) is misspecified, provided the other is correctly specified. This robustness is paramount for real-world machine intelligence applications, where achieving perfect model specification is often challenging due to lack of prior knowledge, data complexity or inherent biases. Furthermore, FOCaL’s flexibility to incorporate arbitrary, state-of-the-art machine learning algorithms for modeling the nuisance functions and the final F-CATE regression allows it to capture complex, non-linear relationships without imposing rigid parametric assumptions. This is crucial for capturing how the entire functional response varies across different subpopulations, and thus provide granular and interpretable causal insights that go beyond simple scalar averages.

We confirmed FOCaL’s superior performance and robustness against existing non-robust functional methods through a comprehensive simulation study, and we demonstrated its practical scope through applications to real-world functional datasets from the SHARE study (Alcser et al., 2005) and from the COVID-19 epidemic in Italy (Boschi et al., 2026). Also importantly, FOCaL possesses theoretical guarantees, including an oracle property and valid simultaneous confidence bands (see Methods and Supplementary Information for details). Such guarantees further solidify FOCaL’s statistical rigor and enable reliable uncertainty quantification for the estimated F-CATE.

Despite its strengths, FOCaL operates under a number of assumptions that are typical in the causal inference and functional data analysis literature. We note that, albeit standard, these assumptions are crucial; their violation could impact the effectiveness of FOCaL, as well as the validity of causal claims. Moreover, while FOCaL’s use of highly flexible machine learning algorithms is a strength, it can also lead to increased computational burden. For the simulations and applications presented in this paper, computational costs

were negligible (in the order of minutes on standard laptops). However, they may escalate in applications with much larger sample sizes or much more densely sampled functional data. Future work could explore more computationally efficient functional regression techniques or distributed computing strategies to enhance scalability.

Looking ahead, our proposal opens several exciting avenues for future research. Extensions could include adapting FOCaL to handle multimodal covariates, which are increasingly common in biomedical and social science applications (Boschi et al., 2024b; Ektefaie et al., 2023; Ngiam et al., 2011). Foundation models may be employed to learn latent embeddings, simultaneously leveraging data with different modalities (curves, images, scalars, labels, etc.) – and thus providing further insights on heterogeneous effects (Bengio et al., 2013; Rajendran et al., 2024). Methods for estimating the effects of time-varying treatments and dynamic treatment regimes on functional outcomes would be another important research direction (Tan et al., 2025). Furthermore, exploring the integration of cutting-edge deep learning architectures specifically designed for functional data within FOCaL’s nuisance function and F-CATE estimation stages could unlock even greater flexibility and predictive power (Rao and Reimherr, 2023a,b).

Ultimately, FOCaL provides a rigorous foundation for applying modern causal learning techniques to the rich data structures increasingly encountered in scientific research, paving the way for more sophisticated and trustworthy AI systems capable of nuanced causal understanding and precision decision-making in personalized health, adaptive policy design, and beyond.

## 4 Methods

### 4.1 Notation and target identification

Let  $\mathcal{T} = [t_1, t_2]$  be a closed bounded interval. Without loss of generality, we shall consider  $\mathcal{T} = [0, 1]$ . Let  $A \in \{0, 1\}$  be a binary variable that indicates whether a subject belongs to the treated group ( $A = 1$ ) or to the control group ( $A = 0$ );  $X \in \mathbb{R}^p$  be a  $p$ -dimensional vector of pretreatment covariates; and  $\mathcal{Y}^{(0)}, \mathcal{Y}^{(1)} \in \mathbb{L}_2(\mathcal{T})$  be square integrable functions defined over  $\mathcal{T}$ , representing the potential outcomes under control and treatment, respectively. A prototypical *full-data* sample is  $\mathcal{D}^F = (X, A, \mathcal{Y}^{(0)}, \mathcal{Y}^{(1)})$ . Of course, in practice, we never have access to  $\mathcal{D}^F$ , as we can only observe one of the two potential outcomes. More formally, we have access to a collection of  $n$  independent and identically distributed *observed-data* samples,  $\{\mathcal{D}_i = (A_i, X_i, \mathcal{Y}_i)\}_{i=1}^n$ , where  $\mathcal{Y}_i = A_i \mathcal{Y}_i^{(1)} + (1 - A_i) \mathcal{Y}_i^{(0)}$  represents the observed outcome. We let  $\mathcal{D} = (A, X, \mathcal{Y})$  denote an independent copy of  $\mathcal{D}_i = (A_i, X_i, \mathcal{Y}_i)$ . Finally, we assume that  $\mathbb{L}_2(\mathcal{T})$ , the space of square integrable functions over  $\mathcal{T}$ , is equipped with the  $\mathbb{L}_2$ -norm defined by  $\|f\|_{\mathbb{L}_2}^2 = \int_{\mathcal{T}} (f(t))^2 dt < \infty$ , for  $f \in \mathbb{L}_2(\mathcal{T})$ , thus making  $(\mathbb{L}_2(\mathcal{T}), \|\cdot\|_{\mathbb{L}_2})$  a Hilbert space. In principle,  $\mathcal{T}$  could be multidimensional, but for simplicity we consider it to be a proper subset of  $\mathbb{R}$ .

Our target is the *functional conditional average treatment effect* (F-CATE), defined as

$$\theta^*(x) = \mathbb{E}[\mathcal{Y}^{(1)} - \mathcal{Y}^{(0)} | X = x], \quad (2)$$

where the expectation is taken over the data generating process. Recall that the potential outcomes  $\mathcal{Y}^{(0)}, \mathcal{Y}^{(1)}$  are functions over  $\mathcal{T}$ ; so is  $\theta^*(x)$  for each  $x \in \mathbb{R}^p$  (we omit arguments over  $\mathcal{T}$  for notational simplicity). To provide some intuition, if  $p = 1$  and thus  $x \in \mathbb{R}$ ,  $\theta^*$  is a surface defined over the domain  $\mathcal{T} \times \mathbb{R}$ , and each evaluation of  $\theta^*$  at  $x$ , i.e.  $\theta^*(x)$ , is a function defined over  $\mathcal{T}$ .

The F-CATE target in Equation 2 is a function of the full data, and as such it is not directly learnable from the observed data. With the following minimal set of assumptions, which are standard in the causal inference literature (Kennedy, 2023; Wager, 2024), we can identify the target relying exclusively on the observed data.

**Assumption 4.1** (Identifiability). Let the following hold:

- a. **Consistency.** The potential outcome under a specific treatment is the same regardless of the mechanism by which the treatment is administered; that is,  $\mathcal{Y} = \mathcal{Y}^{(a)}$  if  $A = a$ . Equivalently,  $\mathcal{Y} = A\mathcal{Y}^{(1)} + (1 - A)\mathcal{Y}^{(0)}$ .

b. **No unmeasured confounding.**  $(\mathcal{Y}^{(0)}, \mathcal{Y}^{(1)}) \perp\!\!\!\perp A | X$ .

c. **Weak positivity.**  $0 < \Pr[A = 1 | X = x] < 1$  for every  $x \in \mathbb{R}^p$  almost surely.

Define the *regression functions* as

$$\mu^{*(a)}(x) = \mathbb{E}[\mathcal{Y} | X = x, A = a], \quad a \in \{0, 1\}, \quad (3)$$

and the *propensity score function* as

$$\pi^*(x) = \Pr[A = 1 | X = x] = \mathbb{E}[\mathbb{1}\{A = 1\} | X = x]. \quad (4)$$

These are usually referred to as *nuisance functions*; note that they depend only on the observed data (Kennedy, 2024). Finally, define the *pseudo-outcomes* as

$$\gamma^{*(1)}(\mathcal{D}) = \mu^{*(1)}(X) + \frac{A}{\pi^*(X)} (\mathcal{Y} - \mu^{*(1)}(X)), \quad \gamma^{*(0)}(\mathcal{D}) = \mu^{*(0)}(X) + \frac{1-A}{1-\pi^*(X)} (\mathcal{Y} - \mu^{*(0)}(X)). \quad (5)$$

The following claim makes the identification of F-CATE explicit.

**Lemma 4.2.** *Under Assumption 4.1 (identifiability), the F-CATE target defined in Eq. 2 can be rewritten as:*

$$\theta^*(x) = \mathbb{E}[\gamma^{*(1)}(\mathcal{D}) - \gamma^{*(0)}(\mathcal{D}) | X = x]. \quad (6)$$

We defer the proof of this and subsequent claims to the Supplementary Information, and are now ready to provide full detail on the proposed FOCaL.

## 4.2 FOCaL in detail

FOCaL is constructed as a doubly robust meta-learner for  $\theta^*(x)$ , building upon the principles of the DR-Learner (Kennedy, 2023) but explicitly extending them to functional outcomes. FOCaL's pipeline comprises three stages: (i) estimation of the nuisance functions, (ii) reconstruction of the functional pseudo-outcomes, and (iii) final estimation of the F-CATE.

In the *first stage*, FOCaL estimates the following nuisance functions:

- **Functional outcome regressions:** these represent the conditional expectations of the functional outcome given the covariates and the treatment status, denoted as  $\mu^{*(a)}(x) = \mathbb{E}[\mathcal{Y} | X = x, A = a]$ ,  $a \in \{0, 1\}$ . They are estimated fitting functional regression models to the observed data (Kokoszka and Reimherr, 2017). We note that other machine learning models, such as specialized neural networks for functional data (Boschi et al., 2024c; Yao et al., 2021), can be employed as base learners for this task. The estimates are denoted as  $\hat{\mu}^{(a)}(x)$ ,  $a \in \{0, 1\}$ .
- **Propensity score:** this represents the probability of receiving treatment given the covariates, denoted as  $\pi^*(x) = \Pr[A = 1 | X = x]$ . Its estimation can employ a variety of models and algorithms for binary classification (e.g., logistic regression, random forests, etc.). The estimate is denoted as  $\hat{\pi}(x)$ .

In the *second stage*, FOCaL reconstructs the functional pseudo-outcomes  $\gamma^{(a)}(\mathcal{D}_i)$ ,  $a \in \{0, 1\}$  for each individual  $i = 1, \dots, n$ . These capture the individual-level treatment effect on the functional outcome. For an individual with observed outcome  $\mathcal{Y}_i$ , covariates  $X_i$  and treatment  $A_i$  the estimates are:

$$\hat{\gamma}^{(1)}(\mathcal{D}_i) = \hat{\mu}^{(1)}(X_i) + \frac{A_i}{\hat{\pi}(X_i)} (\mathcal{Y}_i - \hat{\mu}^{(1)}(X_i)), \quad \hat{\gamma}^{(0)}(\mathcal{D}_i) = \hat{\mu}^{(0)}(X_i) + \frac{1-A_i}{1-\hat{\pi}(X_i)} (\mathcal{Y}_i - \hat{\mu}^{(0)}(X_i)). \quad (7)$$

A fundamental property of this construction, extended to the functional setting, is its double robustness. Double robustness is critical for the reliability of FOCaL estimates, as consistency is maintained even if one of the nuisance models is misspecified, which is a common occurrence in real-world applications. We note that, in applications involving functional outcomes, it would be reasonable to assume that estimation of the regression functions  $\mu^{*(a)}(x)$ ,  $a \in \{0, 1\}$ , is a more complex task than estimation of the propensity score

function  $\pi^*(x)$ . Indeed,  $\mu^{*(a)}(x)$  maps a vector of size  $p$  into a function in  $C(\mathcal{T})$ , while  $\pi^*(x)$  maps the same vector into a variable in  $(0, 1)$ . Double robustness ensures that, if  $\hat{\pi}(x)$  converges to  $\pi^*(x)$ ,  $\hat{\gamma}^{(a)}(\mathcal{D})$  converges to  $\gamma^{*(a)}(\mathcal{D})$  for any choice of  $\hat{\mu}^{(a)}(x)$ . See [Kennedy \(2024\)](#); [Testa et al. \(2025\)](#) for additional information and perspectives on double robustness.

In the *third stage*, FOCaL estimates the F-CATE  $\theta^*(x)$  by fitting a final regression model for the difference between the functional pseudo-outcomes  $\hat{\gamma}^{(1)}(\mathcal{D}) - \hat{\gamma}^{(0)}(\mathcal{D})$  (a functional response) against the covariates  $X$ . This involves again utilizing functional regression techniques. The resulting  $\hat{\theta}(x)$  provides a comprehensive and interpretable map of how the causal effect on the functional outcome varies across the entire covariate space.

To mitigate overfitting of the nuisance functions and ensure valid asymptotic inference for the FOCaL estimator, we employ *cross-fitting* ([Ahrens et al., 2025](#); [Chernozhukov et al., 2018](#)). We randomly split the observations  $\{\mathcal{D}_1, \dots, \mathcal{D}_n\}$  into  $J$  disjoint folds (without loss of generality, assume that  $n$  is divisible by  $J$ ). For each  $j = 1, \dots, J$  we form  $\hat{\mathbb{P}}^{[-j]}$  with all but the  $j$ -th fold, and  $\mathbb{P}_n^{[j]}$  with the  $j$ -th fold. Then, we learn  $\hat{\mu}^{(a)[-j]}(x)$ ,  $a \in \{0, 1\}$  and  $\hat{\pi}^{[-j]}(x)$  using data in  $\hat{\mathbb{P}}^{[-j]}$ , and compute  $\hat{\gamma}_{\hat{\mu}^{(a)[-j]}, \hat{\pi}^{[-j]}}^{(a)}(\mathcal{D})$ ,  $a \in \{0, 1\}$  and regress their difference on  $X$  using data in  $\mathbb{P}_n^{[j]}$ . This produces a fold-specific estimate  $\hat{\theta}^{[j]}(x)$  of the F-CATE. Finally, we average across folds to obtain our cross-fitted FOCaL estimator as

$$\hat{\theta}(x) = \frac{1}{J} \sum_{j=1}^J \hat{\theta}^{[j]}(x). \quad (8)$$

Cross-fitting ensures that the nuisance function estimation underlying the reconstruction of functional pseudo-outcomes for any given observation is always performed on an independent subset of the data. The functional pseudo-outcomes are computed for all observations by iterating this process across all  $J$  folds. This orthogonalization effectively debiases the final F-CATE estimation and allows for full sample efficiency, even when highly flexible machine learning models are used for nuisance function estimation.

### 4.3 Theoretical guarantees and inference

In addition to double robustness, FOCaL enjoys an oracle property if the regression of the difference between functional pseudo-outcomes on the covariates is *stable*, as defined below.

**Definition 4.3** (Stability). *Let  $\hat{\mathbb{P}}^{[-j]}$  and  $\mathbb{P}_n^{[j]}$  be two disjoint sub-samples obtained by randomly splitting observations with cross-fitting. Let:*

- $\hat{f}^{[-j]}(\mathcal{D})$  be an estimate of  $f^*(\mathcal{D})$  based on data in  $\hat{\mathbb{P}}^{[-j]}$ .
- $\hat{b}^{[-j]}(x) = \mathbb{E}[\hat{f}^{[-j]}(\mathcal{D}) - f^*(\mathcal{D}) \mid \hat{\mathbb{P}}^{[-j]}, X = x]$  be the pointwise conditional bias of the estimator  $\hat{f}^{[-j]}$ .
- $\hat{\mathbb{E}}^{[j]}[\cdot \mid X = x]$  be a generic estimator of  $\mathbb{E}[\cdot \mid X = x]$  based on data in  $\mathbb{P}_n^{[j]}$ .

The estimator  $\hat{\mathbb{E}}^{[j]}[\cdot \mid X = x]$  is stable at  $X = x$  with respect to a distance metric  $d$  if

$$\frac{\|\hat{\mathbb{E}}^{[j]}[\hat{f}(\mathcal{D}) \mid X = x] - \hat{\mathbb{E}}^{[j]}[f^*(\mathcal{D}) \mid X = x] - \hat{\mathbb{E}}^{[j]}[\hat{b}^{[-j]}(X) \mid X = x]\|_{\mathbb{L}_2}}{\left\| \sqrt{\mathbb{E}[(\hat{\mathbb{E}}^{[j]}[f^*(\mathcal{D}) \mid X = x] - \mathbb{E}[f^*(\mathcal{D}) \mid X = x])^2]} \right\|_{\mathbb{L}_2}} \xrightarrow{p} 0, \quad (9)$$

whenever  $d(\hat{f}, f^*) \xrightarrow{p} 0$ .

The definition of stability of an estimator was originally introduced by [Kennedy \(2023\)](#) for one-dimensional outcomes; our definition extends it accounting for the infinite-dimensional nature of functional outcomes. Endowed with this definition, we now state the oracle property in the following theorem.

**Theorem 4.4** (Oracle property). *Let  $\hat{\mathbb{P}}^{[-j]}$  and  $\mathbb{P}_n^{[j]}$  be two disjoint sub-samples obtained by randomly splitting observations with cross-fitting. Assume that:*

- The estimator  $\hat{\theta}^{[j]}(x) = \hat{\mathbb{E}}^{[j]} \left[ \hat{\gamma}_{\hat{\mu}^{(1)[\neg j]}, \hat{\pi}^{[\neg j]}}^{(1)}(\mathcal{D}) - \hat{\gamma}_{\hat{\mu}^{(0)[\neg j]}, \hat{\pi}^{[\neg j]}}^{(0)}(\mathcal{D}) \mid X = x \right]$  is stable with respect to a distance  $d$ .
- $d \left( \hat{\gamma}_{\hat{\mu}^{(a)[\neg j]}, \hat{\pi}^{[\neg j]}}^{(a)}(\mathcal{D}), \gamma^{*(a)}(\mathcal{D}) \right) \xrightarrow{p} 0$  for  $a \in \{0, 1\}$ .

Let  $\tilde{\theta}^{[j]}(x) = \hat{\mathbb{E}}^{[j]} \left[ \gamma^{*(1)}(\mathcal{D}) - \gamma^{*(0)}(\mathcal{D}) \mid X = x \right]$  be an oracle estimator that regresses the true difference in pseudo-outcomes on the covariates using data in  $\mathbb{P}_n^{[j]}$ , and denote its risk by

$$\tilde{R}_n^{[j]}(x) = \left\| \sqrt{\mathbb{E} \left[ \left( \hat{\mathbb{E}}^{[j]} \left[ \gamma^{*(1)}(\mathcal{D}) - \gamma^{*(0)}(\mathcal{D}) \mid X = x \right] - \mathbb{E} \left[ \gamma^{*(1)}(\mathcal{D}) - \gamma^{*(0)}(\mathcal{D}) \mid X = x \right] \right)^2 \right]} \right\|_{\mathbb{L}_2}. \quad (10)$$

Then

$$\left\| \hat{\theta}^{[j]}(x) - \tilde{\theta}^{[j]}(x) \right\|_{\mathbb{L}_2} = \left\| \hat{\mathbb{E}}^{[j]} \left[ \hat{b}^{[\neg j]}(X) \mid X = x \right] \right\|_{\mathbb{L}_2} + o_{\mathbb{P}} \left( \tilde{R}_n^{[j]}(x) \right), \quad (11)$$

where

$$\hat{b}^{[\neg j]}(x) = \frac{(\hat{\pi}^{[\neg j]}(x) - \pi^*(x))(\hat{\mu}^{(1)[\neg j]}(x) - \mu^{*[1]}(x))}{\hat{\pi}(x)} + \frac{(\hat{\pi}^{[\neg j]}(x) - \pi^*(x))(\hat{\mu}^{(0)[\neg j]}(x) - \mu^{*[0]}(x))}{1 - \hat{\pi}(x)}. \quad (12)$$

If it further holds that  $\left\| \hat{\mathbb{E}}^{[j]} \left[ \hat{b}^{[\neg j]}(X) \mid X = x \right] \right\|_{\mathbb{L}_2} = o_{\mathbb{P}} \left( \tilde{R}_n^{[j]}(x) \right)$ , then  $\hat{\theta}^{[j]}(x)$  is oracle efficient, i.e. asymptotically equivalent to the oracle estimator  $\tilde{\theta}^{[j]}(x)$  in the sense that

$$\frac{\left\| \hat{\theta}^{[j]}(x) - \tilde{\theta}^{[j]}(x) \right\|_{\mathbb{L}_2}}{\tilde{R}_n^{[j]}(x)} \xrightarrow{p} 0. \quad (13)$$

The previous result is powerful, as it provides strong asymptotic estimation guarantees for FOCaL. Moreover, it has actionable consequences for inferential purposes, as articulated in the following proposition.

**Proposition 4.5** (Valid and simultaneous coverage). *Let  $\hat{\mathbb{P}}^{[\neg j]}$  and  $\mathbb{P}_n^{[j]}$  be two disjoint sub-samples obtained by randomly splitting observations with cross-fitting. Assume:*

- The estimator  $\hat{\theta}^{[j]}(x)$  is stable with respect to a distance  $d$ .
- $d \left( \hat{\gamma}_{\hat{\mu}^{(a)[\neg j]}, \hat{\pi}^{[\neg j]}}^{(a)}(\mathcal{D}), \gamma^{*(a)}(\mathcal{D}) \right) \xrightarrow{p} 0$  for  $a \in \{0, 1\}$ .
- The oracle estimator  $\tilde{\theta}^{[j]}(x)$  has an asymptotic Gaussian process behavior, that is

$$\sqrt{n} \left( \tilde{\theta}^{[j]}(x) - \theta^*(x) \right) \rightsquigarrow \mathcal{GP}(0, \Sigma(x)), \quad (14)$$

$$\text{where } \Sigma(x) = \mathbb{V} \left[ \gamma^{*(1)}(\mathcal{D}) - \gamma^{*(0)}(\mathcal{D}) \mid X = x \right].$$

Then the asymptotic distribution of  $\hat{\theta}^{[j]}(x)$  matches the one of  $\tilde{\theta}^{[j]}(x)$  with  $\hat{\Sigma}(x)$ , where we define  $\hat{\Sigma}(x) = \hat{\mathbb{E}}^{[j]} \left[ \left( \hat{\gamma}_{\hat{\mu}^{(1)[\neg j]}, \hat{\pi}^{[\neg j]}}^{(1)}(\mathcal{D}) - \hat{\gamma}_{\hat{\mu}^{(0)[\neg j]}, \hat{\pi}^{[\neg j]}}^{(0)}(\mathcal{D}) \right) \left( \hat{\gamma}_{\hat{\mu}^{(1)[\neg j]}, \hat{\pi}^{[\neg j]}}^{(1)}(\mathcal{D}) - \hat{\gamma}_{\hat{\mu}^{(0)[\neg j]}, \hat{\pi}^{[\neg j]}}^{(0)}(\mathcal{D}) \right)^T \mid X = x \right]$ .

Thus, for any given covariate profile  $X = x$ , we can provide valid and simultaneous confidence bands through a parametric bootstrap, as proposed by [Pini and Vantini \(2017\)](#). We repeatedly sample from the Gaussian process and estimate quantiles – without any additional assumption on the covariance function. In symbols, the band takes the form  $C_{\alpha}(x) = [\hat{\theta}_{\alpha/2}(x), \hat{\theta}_{1-\alpha/2}(x)]$ , where  $\hat{\theta}_{\alpha/2}(x)$  and  $\hat{\theta}_{1-\alpha/2}(x)$  indicate the estimated  $\alpha/2$  and  $1 - \alpha/2$  quantiles, respectively. Given its ease of implementation, and the fact that it requires no additional assumptions, we adopt this parametric bootstrap approach for evaluating uncertainty in FOCaL results.

#### 4.4 Simulation study

To rigorously assess the performance of FOCaL in synthetic scenarios, we design a simulation experiment involving  $n = 5000$  independent observations with functional outcomes observed on a dense grid of 100 equidistant points over the domain  $\mathcal{T} = [0, 1]$ .

We first generate four baseline covariates  $X_1, X_2, X_3, X_4$  from a standard multivariate normal distribution  $\mathcal{N}(0, I_4)$ . Treatment assignment  $A_i \in \{0, 1\}$  is drawn from a Bernoulli distribution with propensity scores  $\pi^*(X_1, X_2, X_3, X_4) = \text{logit}^{-1}(\eta(X_1, X_2, X_3, X_4))$ , where the inverse logit function is defined as  $\text{logit}^{-1}(x) = 1/(1 + \exp(-x))$  and the linear function  $\eta(X_1, X_2, X_3, X_4) = -X_1 + 0.5X_2 - 0.25X_3 - 0.1X_4$  creates a strong dependency on the baseline covariates. The functional regression functions are generated using a time-varying coefficient model, that is:

$$\mu^{*(a)}(X_1, X_2, X_3, X_4) = \beta_0 + \sum_{j=1}^4 \beta_j X_j + \delta(a) \beta_5 X_1, \quad (15)$$

where  $\delta(a) = 1$  if  $a = 1$  and 0 otherwise, and the  $\beta_j$ 's depend on  $t \in \mathcal{T}$ . Specifically, to ensure realistic smoothness and correlation structures, the coefficients  $\beta_j$  are sampled from a Gaussian Process with Matérn covariance kernel defined, for any  $t, s \in \mathcal{T}$ , as:

$$C(s, t) = \frac{\alpha^2}{\Gamma(\nu) 2^{\nu-1}} \left( \frac{\sqrt{2\nu}}{l} |s - t| \right)^\nu \chi_\nu \left( \frac{\sqrt{2\nu}}{l} |s - t| \right). \quad (16)$$

Here  $\chi_\nu$  is a modified Bessel function, and we set the parameters to  $l = 0.25$ ,  $\nu = 5.5$ ,  $\alpha = 2$  for  $\beta_1, \dots, \beta_4$  and  $\alpha = 10$  for  $\beta_5$ . Then, for each observation  $i = 1, \dots, n$ , we define potential outcomes as

$$\mathcal{Y}_i^{(a)} = \mu^{*(a)}(X_{i1}, X_{i2}, X_{i3}, X_{i4}) + \varepsilon_i, \quad a \in \{0, 1\}, \quad (17)$$

where the noise term  $\varepsilon$  is drawn from a Gaussian Process with Matérn covariance kernel ( $l = 0.25$ ,  $\nu = 5.5$ ,  $\alpha = 10$ ). Finally, for each observation  $i = 1, \dots, n$ , the observed functional outcome is

$$\mathcal{Y}_i = A_i \mathcal{Y}_i^{(1)} + (1 - A_i) \mathcal{Y}_i^{(0)}. \quad (18)$$

This construction induces a heterogeneous treatment effect driven by  $X_1$  and  $\beta_5$ , resulting in a non-trivial F-CATE target  $\theta^*(x)$ .

To control the degree of model misspecification, we also define the non-linear transformations  $Z_1, Z_2, Z_3, Z_4$  of the covariates  $X_1, X_2, X_3, X_4$  defined as

$$Z_1 = \exp(X_1/2), \quad Z_2 = \frac{X_2}{1 + \exp(X_1)} + 10, \quad Z_3 = \left( \frac{X_1 X_3}{25} + 0.6 \right)^3, \quad Z_4 = (X_2 + X_4 + 20)^2. \quad (19)$$

An analyst who fits a linear model for the outcome or a logistic model for the propensity score using the covariates  $Z_1, Z_2, Z_3, Z_4$  will have a misspecified model. A correct specification would require the analyst to know the true latent variables  $X_1, X_2, X_3, X_4$  or the exact inverse transformations. In all cases, 5-fold cross-fitting is used. We thus consider four scenarios:

1. Correct specification: both nuisance models are correctly specified;
2. Misspecified regression function: only  $\hat{\mu}^{(a)}$  is misspecified by injecting the non-linear transformation through  $Z_1, Z_2, Z_3, Z_4$ ;
3. Misspecified propensity score: only  $\hat{\pi}$  is misspecified by injecting the non-linear transformation through  $Z_1, Z_2, Z_3, Z_4$ ;
4. Fully misspecified:  $\hat{\mu}^{(a)}$  and  $\hat{\pi}$  are both misspecified.

This design allows us to empirically assess the double robustness property of FOCaL: consistency is preserved if at least one nuisance model is correctly specified, and deteriorates only under joint misspecification.

We repeat the simulation experiment described above 5000 times. For each scenario, we compute the aggregated root mean squared error (ARMSE) between the estimated functional treatment effect  $\hat{\theta}$  and the ground truth  $\theta^*(x)$ , where  $\text{ARMSE}(\hat{\theta}, \theta^*) = \int_x \|\hat{\theta}(x) - \theta^*(x)\|_{\mathbb{L}_2} dx$ . This metric provides a direct and interpretable measure of estimation accuracy across the covariate space, as well as time through the  $\mathbb{L}_2$  norm.

## 4.5 SHARE study

SHARE (*Survey of Health, Aging and Retirement in Europe*) is a research infrastructure that aims to investigate the effects of health, social, economic and environmental policies on the life course of European citizens (Bergmann et al., 2017; Börsch-Supan, 2020; Börsch-Supan et al., 2013). We preprocess data following the steps described in Boschi et al. (2024a). We focus on the 1518 subjects who participated in at least seven out of the eight waves (i.e., survey times). We investigate a subset of the variables from the EasySHARE dataset (Gruber et al., 2014), a preprocessed version of the SHARE data. While some of these variables are characterized by values that change over time (e.g., CASP and mobility index) and are suitable for a functional representation, others are scalar (e.g., education years) or categorical (e.g., gender) and do not evolve across waves. We smooth time-varying variables using cubic *B-splines* with knots at each survey date and roughness penalty on the curves second derivative (Ramsay and Silverman, 2005). For each curve, the smoothing parameter is selected by minimizing the average generalized cross-validation error (Craven and Wahba, 1978). Note that, although survey dates and number of measurements may vary across subjects, creating a functional representation provides a natural imputation for missing values and facilitates the comparison of different statistical units across the entire temporal domain.

For this application, FOCaL employs neural networks for the regression nuisance function and the pseudo-outcome regression, and a logistic regression for the propensity score nuisance function. For the regression nuisance function, we opt for a two-layer neural network (10 neurons per layer) with adaptive learning rate and 50k iterations. For the pseudo-outcome regression we opt for a simpler, one-layer neural network with 5 neurons to encourage smoothness. A small Ridge penalization ( $1e^{-3}$ ) is added for regularization. We employ cross-fitting with 5 balanced folds.

## 4.6 COVID-19 study

This study investigates mortality data at the provincial level for the two pre-vaccine COVID 19 waves that occurred in Italy in 2020-2021. Specifically, we consider differential mortality for 107 provinces, computed for a total of 300 longitudinal points (150 days for each wave), as provided by Boschi et al. (2026). In addition to mortality, we consider a set of covariates describing some key socio-economic, demographic and infrastructural indicators for each province. To define our treatment  $A$ , we binarize one such covariate; namely, the ratio between adults and family doctors, as observed for each province in 2019. Using the national median as a cut point, we consider as “treated” provinces above the median (poor distributed primary health care;  $A = 1$ ) and as “untreated” provinces below the median (better distributed primary health care;  $A = 0$ ).

Estimates of the nuisance functions and the pseudo-outcome regression are obtained as in the SHARE application (neural networks for the regression nuisance function and the pseudo-outcome regression, and logistic regression for the propensity score nuisance function). Here though both neural networks are three-layered – the former with 20 neurons per layer and the latter with 10 neurons per layer, both with “relu” activation function and Ridge penalization. Again, FOCaL is run via a 5-fold cross-fit.

To obtain FATE estimates, we take the average over the pseudo-outcome curves, trimming the top 1% observations showing the largest norms. To compute  $\hat{\Sigma}$  as in Proposition 4.5, which is required to build confidence bands of F-CATE surface cuts, we employ a multi-output random forest regression model (100 trees, 200 minimum samples per leaf). Evaluating the fitted model at any specific  $x$  yields  $\hat{\Sigma}(x)$ .

## Data availability

Due to data-sharing restrictions, we cannot release the data used in our SHARE application. However, access to data from the SHARE study can be freely requested through the official portal at <https://share-eric.eu/data>. Data for our COVID-19 application are available at <https://github.com/tobiaboschi/fdaCOVID2>.

## Code availability

The implementation code for FOCaL, as well as the code needed to reproduce the simulation study and the applications presented in this paper, is available on GitHub at <https://github.com/testalorenzo/FOCaL>.

## Acknowledgments

L.T. wishes to thank Edward Kennedy and the Causal Inference Reading Group at Carnegie Mellon for helpful discussions. The work of F.C. was partially supported by the Huck Institutes of the Life Sciences at Penn State, the L'EMbeDS Department of Excellence of the Sant'Anna School of Advanced Studies, and the SMaRT CONSTRUCT project (CUP J53C24001460006, as part of FAIR, PE0000013, CUP B53C22003630006, Italian National Recovery and Resilience Plan funded by NextGenerationEU).

## Author contributions

All authors conceived ideas and designed the proposed method. F.S. and L.T. retrieved and processed data and implemented pipelines. All authors participated to the writing of the manuscript. F.C. supervised the research.

## Competing interests

The authors declare no competing interests.

## References

Achim Ahrens, Victor Chernozhukov, Christian Hansen, Damian Kozbur, Mark Schaffer, and Thomas Wiemann. An introduction to double/debiased machine learning. *arXiv preprint arXiv:2504.08324*, 2025.

Kirsten H. Alcser, Grant Benson, Axel Barsch-Supan, Agar Brugiavini, Dimitrios Christelis, Enrica Croda, Marcel Das, Giuseppe de Luca, Janet Harkness, Patrik Hesselius, Tullio Jappelli, Hendrik Jarges, Adriaan Kalwij, Marie-Louise Kemperman, Anders Klevmarken, Oliver Lipps, Omar Paccagnella, Mario Padula, Franco Perrachi, Roberta Rainato, Arthur van Soest, Bengt Swensson, Corrie Vis, Guglielmo Weber, and Bas Weerman. *The Survey of Health, Aging, and Retirement in Europe: Methodology*. Mannheim Research Institute for the Economics of Aging (MEA), 2005.

Abdulfattah S Alqahtani and Aqeel M Alenazi. Stepping towards health: A cross-sectional study of hypertension, mobility, and endurance among saudi adults aged 50 years and older. *Journal of Clinical Medicine*, 14(23):8521, 2025.

Gunnar H Anderson. Effect of age on hypertension: analysis of over 4,800 referred hypertensive patients. *Saudi Journal of Kidney Diseases and Transplantation*, 10(3):286–297, 1999.

Yoshua Bengio, Aaron Courville, and Pascal Vincent. Representation learning: A review and new perspectives. *IEEE transactions on pattern analysis and machine intelligence*, 35(8):1798–1828, 2013.

Michael Bergmann, Thorsten Kneip, Giuseppe De Luca, and Annette Scherpenzeel. Survey participation in the survey of health, ageing and retirement in europe (share), wave 1-6. *Munich: Munich Center for the Economics of Aging*, 2017.

Axel Börsch-Supan. Survey of health, ageing and retirement in europe (share) wave 5. *Release version, 7 (0)*, 2020.

Axel Börsch-Supan, Martina Brandt, Christian Hunkler, Thorsten Kneip, Julie Korbmacher, Frederic Malter, Barbara Schaan, Stephanie Stuck, and Sabrina Zuber. Data resource profile: the survey of health, ageing and retirement in europe (share). *International journal of epidemiology*, 42(4):992–1001, 2013.

Tobia Boschi, Jacopo Di Iorio, Lorenzo Testa, Marzia A Cremona, and Francesca Chiaromonte. Functional data analysis characterizes the shapes of the first covid-19 epidemic wave in italy. *Scientific reports*, 11: 17054, 2021.

Tobia Boschi, Francesca Bonin, Rodrigo Ordóñez-Hurtado, Alessandra Pascale, and Jonathan P Epperlein. A new computationally efficient algorithm to solve feature selection for functional data classification in high-dimensional spaces. In *Forty-first International Conference on Machine Learning*, 2024a.

Tobia Boschi, Francesca Bonin, Rodrigo Ordóñez-Hurtado, Cécile Rousseau, Alessandra Pascale, and John Dinsmore. Functional graph convolutional networks: A unified multi-task and multi-modal learning framework to facilitate health and social-care insights. *arXiv preprint arXiv:2403.10158*, 2024b.

Tobia Boschi, Francesca Bonin, Rodrigo Ordóñez-Hurtado, Cécile Rousseau, Alessandra Pascale, and John Dinsmore. Functional graph convolutional networks: A unified multi-task and multi-modal learning framework to facilitate health and social-care insights. In *Proceedings of the Thirty-Third International Joint Conference on Artificial Intelligence, IJCAI-24*, pages 7188–7196. International Joint Conferences on Artificial Intelligence Organization, 2024c.

Tobia Boschi, Lorenzo Testa, Francesca Chiaromonte, and Matthew Reimherr. Fasten: an efficient adaptive method for feature selection and estimation in high-dimensional functional regressions. *Journal of Computational and Graphical Statistics*, pages 1–24, 2024d.

Tobia Boschi, Jacopo Di Iorio, Lorenzo Testa, Marzia A Cremona, and Francesca Chiaromonte. Contrasting pre-vaccine covid-19 waves in italy through functional data analysis. *Scientific reports*, 16:222, 2026.

Vicki L Burt, Paul Whelton, Edward J Roccella, Clarice Brown, Jeffrey A Cutler, Millicent Higgins, Michael J Horan, and Darwin Labarthe. Prevalence of hypertension in the us adult population: results from the third national health and nutrition examination survey, 1988–1991. *Hypertension*, 25(3):305–313, 1995.

João Caldeira and Hudson Torrent. Forecasting the us term structure of interest rates using nonparametric functional data analysis. *Journal of Forecasting*, 36(1):56–73, 2017.

Alberto Caron, Gianluca Baio, and Ioanna Manolopoulou. Estimating individual treatment effects using non-parametric regression models: A review. *Journal of the Royal Statistical Society Series A: Statistics in Society*, 185(3):1115–1149, 2022.

Victor Chernozhukov, Denis Chetverikov, Mert Demirer, Esther Duflo, Christian Hansen, Whitney Newey, and James Robins. Double/debiased machine learning for treatment and structural parameters, 2018.

Peter Craven and Grace Wahba. Smoothing noisy data with spline functions. *Numerische mathematik*, 31 (4):377–403, 1978.

Marzia A Cremona, Alessia Pini, Fabio Cumbo, Kateryna D Makova, Francesca Chiaromonte, and Simone Vantini. Iwtomics: testing high-resolution sequence-based ‘omics’ data at multiple locations and scales. *Bioinformatics*, 34(13):2289–2291, 2018.

Marzia A Cremona, Lyubov Doroshenko, and Federico Severino. Functional motif discovery in stock market prices. *Available at SSRN 4642040*, 2023.

Jeffrey A Cutler, Paul D Sorlie, Michael Wolz, Thomas Thom, Larry E Fields, and Edward J Roccella. Trends in hypertension prevalence, awareness, treatment, and control rates in united states adults between 1988–1994 and 1999–2004. *Hypertension*, 52(5):818–827, 2008.

Jin-Hong Du, Maya Shen, Hansruedi Mathys, and Kathryn Roeder. Causal differential expression analysis under unmeasured confounders with causarray. *bioRxiv*, pages 2025–01, 2025.

Kreske Ecker, Xavier de Luna, and Lina Schelin. Causal inference with a functional outcome. *Journal of the Royal Statistical Society Series C: Applied Statistics*, 73(1):221–240, 2024.

Yasha Ektefaie, George Dasoulas, Ayush Noori, Maha Farhat, and Marinka Zitnik. Multimodal learning with graphs. *Nature Machine Intelligence*, 5(4):340–350, 2023.

Christian Esposito, Marco Gortan, Lorenzo Testa, Francesca Chiaromonte, Giorgio Fagiolo, Andrea Mina, and Giulio Rossetti. Venture capital investments through the lens of network and functional data analysis. *Applied Network Science*, 7(1):42, 2022.

Bethany Everett and Anna Zajacova. Gender differences in hypertension and hypertension awareness among young adults. *Biodemography and social biology*, 61(1):1–17, 2015.

Stefan Gruber, Christian Hunkler, and Stephanie Stuck. Generating easyshare: guidelines, structure, content and programming. Technical report, SHARE Working Paper Series 17-2014. Munich, 2014.

Sharonne N Hayes and Sandra J Taler. Hypertension in women: current understanding of gender differences. In *Mayo clinic proceedings*, volume 73, pages 157–165. Elsevier, 1998.

Martin Hyde, Richard D Wiggins, Paul Higgs, and David B Blane. A measure of quality of life in early old age: the theory, development and properties of a needs satisfaction model (casp-19). *Aging & mental health*, 7(3):186–194, 2003.

Francesca Ieva, Nicole Fontana, Carlo Andrea Pivato, Emanuele Di Angelantonio, and Piercesare Secchi. Enhancing causal inference in functional data: a method for estimating time-varying causal treatment effects. In *International Workshop on Functional and Operatorial Statistics*, pages 285–293. Springer, 2025.

Guido W Imbens. Causal inference in the social sciences. *Annual Review of Statistics and Its Application*, 11, 2024.

Yujin Jeong, Emily Fox, and Ramesh Johari. Identifying sparse treatment effects. *arXiv preprint arXiv:2404.14644*, 2024.

Edward H Kennedy. Towards optimal doubly robust estimation of heterogeneous causal effects. *Electronic Journal of Statistics*, 17(2):3008–3049, 2023.

Edward H Kennedy. Semiparametric doubly robust targeted double machine learning: a review. *Handbook of statistical methods for precision medicine*, pages 207–236, 2024.

Piotr Kokoszka and Matthew Reimherr. *Introduction to functional data analysis*. CRC Press, 2017.

Xijia Liu, Kreske Ecker, Lina Schelin, and Xavier de Luna. Double robust estimation of functional outcomes with data missing at random. *arXiv preprint arXiv:2411.17224*, 2024.

Donald M Lloyd-Jones, Jane C Evans, and Daniel Levy. Hypertension in adults across the age spectrum: current outcomes and control in the community. *Jama*, 294(4):466–472, 2005.

Aleksander Molak. *Causal Inference and Discovery in Python: Unlock the secrets of modern causal machine learning with DoWhy, EconML, PyTorch and more*. Packt Publishing Ltd, 2023.

Jiquan Ngiam, Aditya Khosla, Mingyu Kim, Juhan Nam, Honglak Lee, Andrew Y Ng, et al. Multimodal deep learning. In *ICML*, volume 11, pages 689–696, 2011.

Yechiam Ostchega, Charles F Dillon, Jeffery P Hughes, Margaret Carroll, and Sarah Yoon. Trends in hypertension prevalence, awareness, treatment, and control in older us adults: data from the national health and nutrition examination survey 1988 to 2004. *Journal of the American Geriatrics Society*, 55(7):1056–1065, 2007.

Alessia Pini and Simone Vantini. Interval-wise testing for functional data. *Journal of Nonparametric Statistics*, 29(2):407–424, 2017.

Mattia Prosperi, Yi Guo, Matt Sperrin, James S Koopman, Jae S Min, Xing He, Shannan Rich, Mo Wang, Iain E Buchan, and Jiang Bian. Causal inference and counterfactual prediction in machine learning for actionable healthcare. *Nature Machine Intelligence*, 2(7):369–375, 2020.

Xin Qi and Ruiyan Luo. Function-on-function regression with thousands of predictive curves. *Journal of Multivariate Analysis*, 163:51–66, 2018.

Goutham Rajendran, Simon Buchholz, Bryon Aragam, Bernhard Schölkopf, and Pradeep Ravikumar. Learning interpretable concepts: Unifying causal representation learning and foundation models. *arXiv preprint arXiv:2402.09236*, 2024.

James O. Ramsay and B. W. Silverman. *Functional data analysis*. Springer, 2 edition, 2005.

Aniruddha Rajendra Rao and Matthew Reimherr. Modern non-linear function-on-function regression. *Statistics and Computing*, 33(6):130, 2023a.

Aniruddha Rajendra Rao and Matthew Reimherr. Nonlinear functional modeling using neural networks. *Journal of Computational and Graphical Statistics*, 32(4):1248–1257, 2023b.

Yordan P Raykov, Hengrui Luo, Justin D Strait, and Wasiur R KhudaBukhsh. Kernel-based estimators for functional causal effects. *arXiv preprint arXiv:2503.05024*, 2025.

Donald B Rubin. Estimating causal effects of treatments in randomized and nonrandomized studies. *Journal of educational Psychology*, 66(5):688, 1974.

Donald B Rubin. Causal inference using potential outcomes: Design, modeling, decisions. *Journal of the American statistical Association*, 100(469):322–331, 2005.

Kathryn Sandberg and Hong Ji. Sex differences in primary hypertension. *Biology of sex differences*, 3(1):7, 2012.

Ruoxu Tan, Wei Huang, Zheng Zhang, and Guosheng Yin. Causal effect of functional treatment. *Journal of Machine Learning Research*, 26(91):1–39, 2025.

Lorenzo Testa, Tobia Boschi, Francesca Chiaromonte, Edward H Kennedy, and Matthew Reimherr. Doubly-robust functional average treatment effect estimation. *arXiv preprint arXiv:2501.06024*, 2025.

Anastasios A Tsiatis. *Semiparametric theory and missing data*, volume 4. Springer, 2006.

Hal R Varian. Causal inference in economics and marketing. *Proceedings of the National Academy of Sciences*, 113(27):7310–7315, 2016.

Cristiana Vitale, Massimo Fini, Giuseppe Speziale, and Sergio Chierchia. Gender differences in the cardiovascular effects of sex hormones. *Fundamental & clinical pharmacology*, 24(6):675–685, 2010.

Stefan Wager. Causal inference: A statistical learning approach, 2024.

Qi Xu, Haoda Fu, and Annie Qu. Optimal individualized treatment rule for combination treatments under budget constraints. *Journal of the Royal Statistical Society Series B: Statistical Methodology*, 86(3):714–741, 2024.

Junwen Yao, Jonas Mueller, and Jane-Ling Wang. Deep learning for functional data analysis with adaptive basis layers. In *International conference on machine learning*, pages 11898–11908. PMLR, 2021.

## Supplementary Information

### A Technical Lemmas

**Lemma A.1.** *If  $|X_n| \xrightarrow{p} 0$ , then  $X_n \xrightarrow{p} 0$ .*

*Proof.* We want to show that

$$\lim_{n \rightarrow \infty} \Pr[|X_n - 0| \geq \varepsilon] = 0, \quad (20)$$

where  $\varepsilon$  is a positive constant. By definition of convergence in probability of  $|X_n|$  to 0, we have that

$$\lim_{n \rightarrow \infty} \Pr[||X_n| - 0| \geq \varepsilon] = 0, \quad (21)$$

where  $\varepsilon$  is a positive constant. Now it is easy to notice that

$$\Pr[||X_n| - 0| \geq \varepsilon] = \Pr[|X_n - 0| \geq \varepsilon], \quad (22)$$

from which the result follows.  $\square$

### B Proofs of main statements

#### B.1 Proof of Lemma 4.2

*Proof.* We start by showing that  $\mathbb{E}[\mathcal{Y}^{(1)} | X = x] = \mathbb{E}[\gamma^{*(1)}(\mathcal{D}) | X = x]$ . This is done exploiting the identifiability Assumptions 4.1. Indeed

$$\begin{aligned} \mathbb{E}[\gamma^{(1)}(\mathcal{D}) | X = x] &= \mathbb{E}\left[\mu^{*(1)}(X) + \frac{A}{\pi^*(X)}(\mathcal{Y} - \mu^{*(1)}(X)) | X = x\right] \\ &= \mathbb{E}[\mu^{*(1)}(X) | X = x] + \mathbb{E}\left[\frac{A}{\pi^*(X)}(\mathcal{Y} - \mu^{*(1)}(X)) | X = x\right] \\ &= \mathbb{E}[\mathbb{E}[\mathcal{Y} | X, A = 1] | X = x] + \mathbb{E}\left[\frac{A}{\pi^*(X)}(\mathcal{Y} - \mu^{*(1)}(X)) | X = x\right] \\ &= \mathbb{E}[\mathbb{E}[\mathcal{Y} | X, A = 1] | X = x] \\ &= \mathbb{E}[\mathcal{Y}^{(1)} | X = x]. \end{aligned} \quad (23)$$

A similar computation leads to  $\mathbb{E}[\mathcal{Y}^{(0)} | X = x] = \mathbb{E}[\gamma^{*(0)}(\mathcal{D}) | X = x]$ . Combining the two results implies the desired equality.  $\square$

#### B.2 Proof of Theorem 4.4

*Proof.* First, we show the conditional bias decomposition. By iterated expectations, it holds that

$$\begin{aligned} \hat{b}^{[-j]}(x) &= \left(\frac{\pi^*(x)}{\hat{\pi}^{[-j]}(x)} - 1\right)(\mu^{*(1)} - \hat{\mu}^{(1)[-j]}(x)) - \left(\frac{1 - \pi^*(x)}{1 - \hat{\pi}^{[-j]}(x)} - 1\right)(\mu^{*(0)} - \hat{\mu}^{(0)[-j]}(x)) \\ &= \frac{(\hat{\pi}^{[-j]}(x) - \pi^*(x))(\hat{\mu}^{(1)[-j]}(x) - \mu^{*[1]}(x))}{\hat{\pi}(x)} + \frac{(\hat{\pi}^{[-j]}(x) - \pi^*(x))(\hat{\mu}^{(0)[-j]}(x) - \mu^{*[0]}(x))}{1 - \hat{\pi}(x)}. \end{aligned} \quad (24)$$

Now, the assumption of stability implies that

$$\frac{\|\hat{\theta}^{[j]}(x) - \tilde{\theta}^{[j]}(x) - \hat{\mathbb{E}}^{[j]}[\hat{b}^{[-j]}(X) | X = x]\|_{\mathbb{L}_2}}{\tilde{R}_n^{[j]}(x)} \xrightarrow{p} 0. \quad (25)$$

By reverse triangle inequality, we know that

$$\|\hat{\theta}^{[j]}(x) - \tilde{\theta}^{[j]}(x) - \hat{\mathbb{E}}^{[j]}[\hat{b}^{[-j]}(X) | X = x]\|_{\mathbb{L}_2} \geq \left| \|\hat{\theta}^{[j]}(x) - \tilde{\theta}^{[j]}\|_{\mathbb{L}_2}(x) - \|\hat{\mathbb{E}}^{[j]}[\hat{b}^{[-j]}(X) | X = x]\|_{\mathbb{L}_2} \right|, \quad (26)$$

which by Squeeze Theorem in turn implies

$$\frac{\left| \|\hat{\theta}^{[j]}(x) - \tilde{\theta}^{[j]}(x)\|_{\mathbb{L}_2} - \|\hat{\mathbb{E}}^{[j]}[\hat{b}^{[-j]}(X) | X = x]\|_{\mathbb{L}_2} \right|}{\tilde{R}_n^{[j]}(x)} \xrightarrow{p} 0. \quad (27)$$

Combined with Lemma A.1 and consistency, this can be written as

$$\|\hat{\theta}^{[j]}(x) - \tilde{\theta}^{[j]}(x)\|_{\mathbb{L}_2} = \|\hat{\mathbb{E}}^{[j]}[\hat{b}^{[-j]}(X) | X = x]\|_{\mathbb{L}_2} + o_{\mathbb{P}}(R_n^{[j]}(x)). \quad (28)$$

If  $\|\hat{\mathbb{E}}^{[j]}[\hat{b}^{[-j]} | X = x]\|_{\mathbb{L}_2} = o_{\mathbb{P}}(\tilde{R}_n^{[j]}(x))$ , the result follows.  $\square$

### B.3 Proof of Proposition 4.5

*Proof.* Stability and  $d\left(\hat{\gamma}_{\hat{\mu}^{(a)}[-j], \hat{\pi}^{[-j]}}^{(a)}(\mathcal{D}), \gamma^{*(a)}(\mathcal{D})\right) \xrightarrow{p} 0$  for  $a \in \{0, 1\}$  together imply that  $\hat{\Sigma}(x) \xrightarrow{p} \Sigma(x)$ . Therefore, by Slutsky theorem, the result follows.  $\square$

## C Additional details on simulations

Ground-truth FCATE surface along  $X_0$  and Time

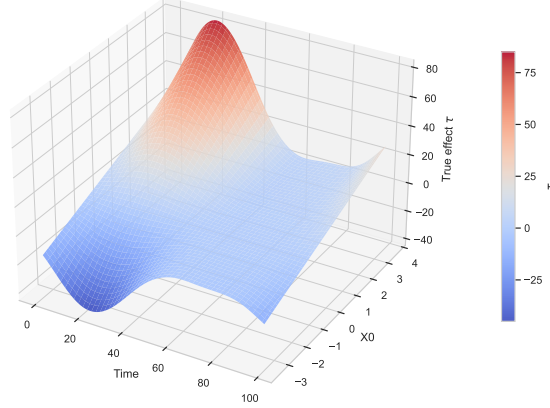


**Figure C.1:** Ground truth F-CATE surface for simulation study. This surface represents the true Functional Conditional Average Treatment Effect (F-CATE) used as the target for one run of the simulation experiments. It is visualized as a function of the functional domain (Time) and the primary covariate of interest ( $X_0$ ), illustrating the complex, non-linear heterogeneity the FOCaL framework is designed to recover.

## D Additional details on real-data applications

### D.1 SHARE study

**Table D.1:** Variables employed in the SHARE application study.

Variable name	Type	Usage
Hypertension condition	Binary	Treatment
High cholesterol	Binary	Treatment
Age	Scalar	Covariate
Years of education	Scalar	Covariate
Number of children	Scalar	Covariate
Gender	Binary	Covariate
Smoke	Binary	Covariate
Vaccinations during childhood	Binary	Covariate
Mobility index	Functional	Outcome
CASP	Functional	Outcome

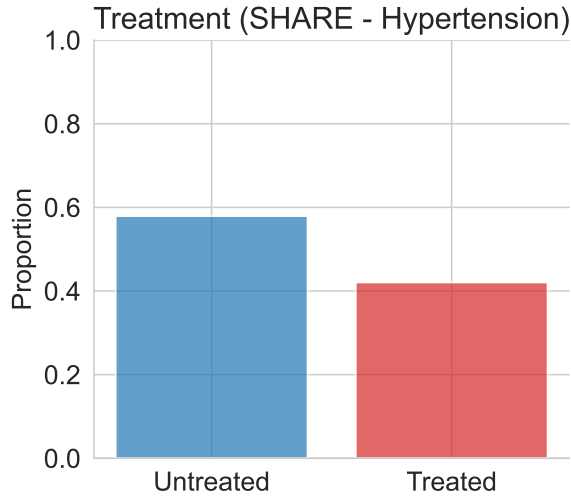


**Figure D.2:** Distribution of treatment status for the SHARE hypertension study. Bar chart showing the proportion of subjects who presented with hypertension at the beginning of the study (Treated,  $n = 419$ ) compared to those who remained healthy throughout the observation window (Untreated,  $n = 577$ ).

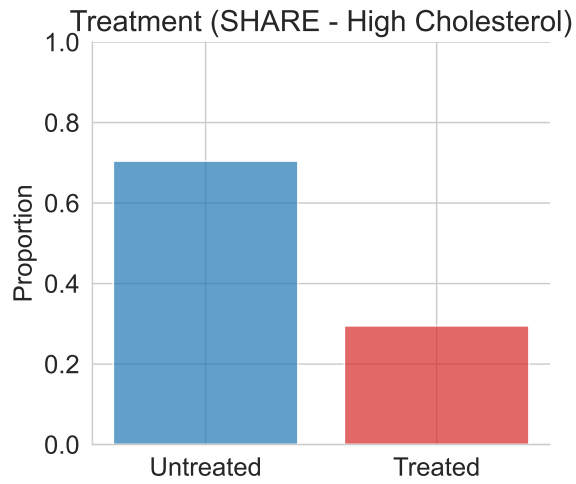


**Figure D.3:** Distribution of treatment status for the SHARE high cholesterol study. Bar chart illustrating the proportion of subjects in the treated (high cholesterol,  $n = 313$ ) and untreated ( $n = 747$ ) cohorts for the secondary SHARE application.

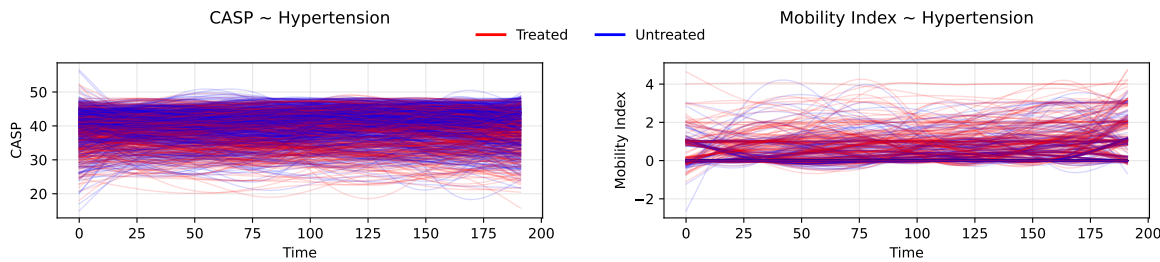


**Figure D.4:** Observed CASP and mobility index functional outcome trajectories for the hypertension cohort (SHARE).

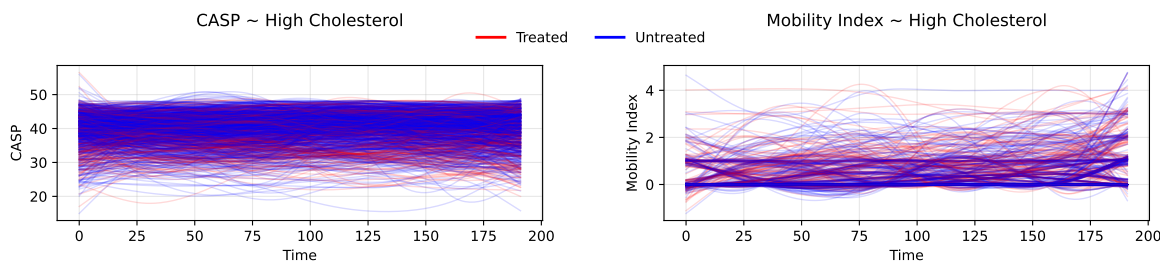


**Figure D.5:** Observed CASP and mobility index functional outcome trajectories for the high cholesterol cohort (SHARE).

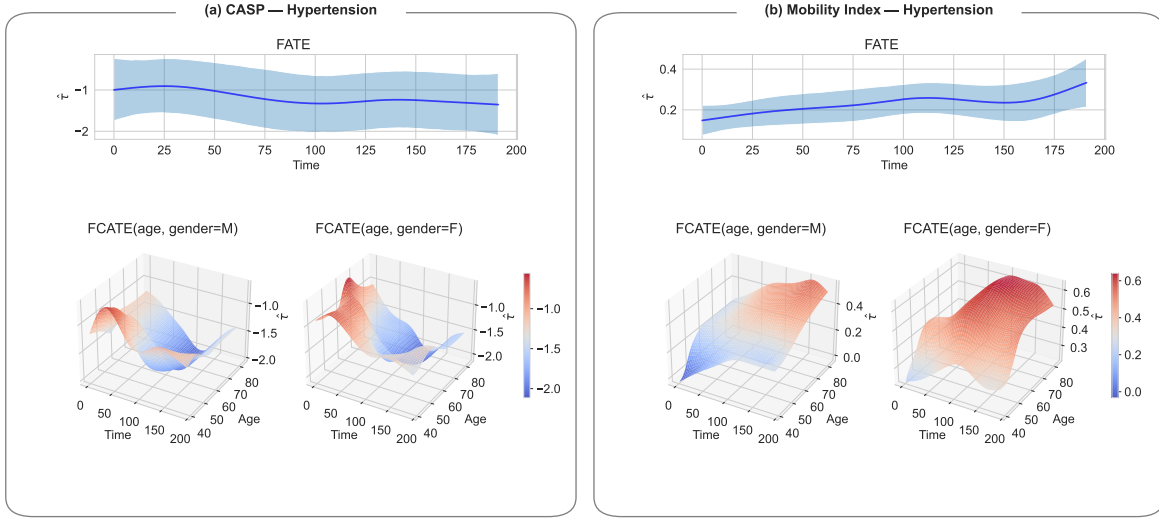


**Figure D.6:** Additional results for the impact of hypertension on quality of life. Compared to Figure 3, here we set the conditioning variable education to a lower quantile (0.2), keeping all other binary and scalar covariates at their modal and mean values, respectively.

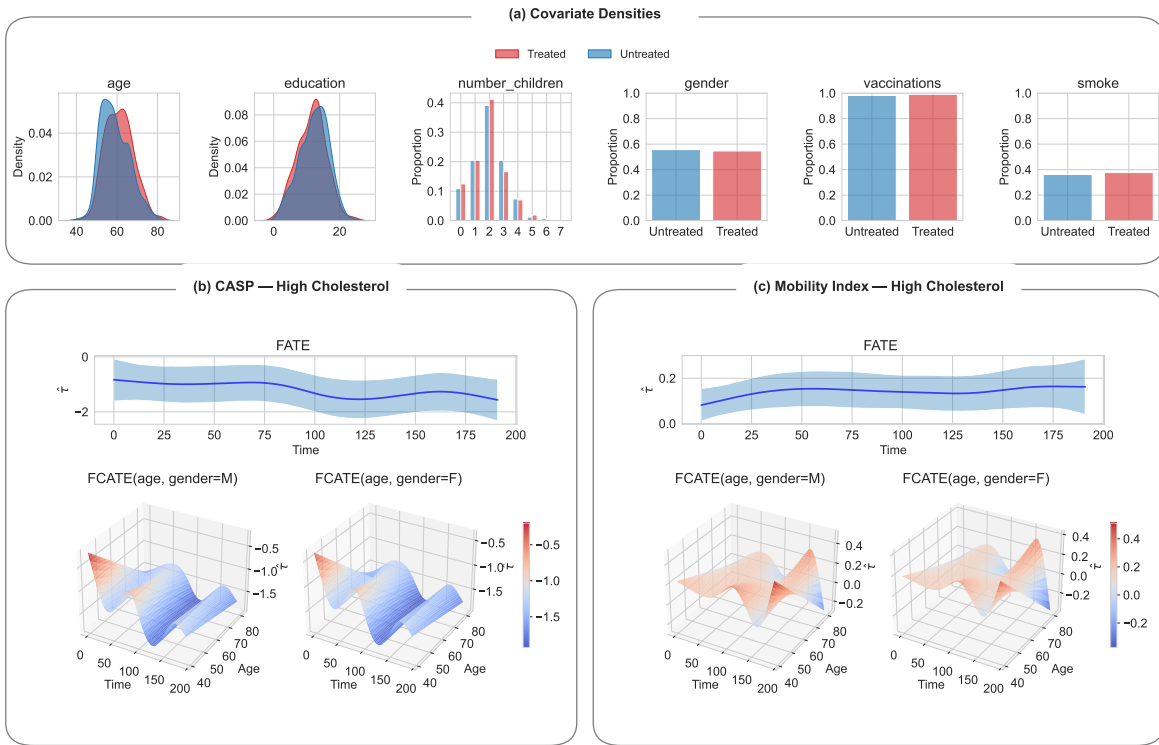


**Figure D.7:** Heterogeneous impact of high cholesterol on quality of life trajectories (SHARE study). Panels can be interpreted as in Figure 3. Note: the plots for CASP and the Mobility Index have response-specific vertical scales (the two outcomes are measured on different scales; see Supplementary Figure D.5).

## D.2 COVID-19 study

**Table D.2:** Variables employed in the COVID-19 application study.

Variable name	Type	Usage
Distributed primary health care (number of adults per family doctor)	Binary	Treatment
Area before	Scalar	Covariate
Percentage of population over 65	Scalar	Covariate
Average beds per hospital	Scalar	Covariate
Average students per classroom	Scalar	Covariate
Average employees per firm	Scalar	Covariate
PM10	Scalar	Covariate
Mortality rate	Functional	Outcome

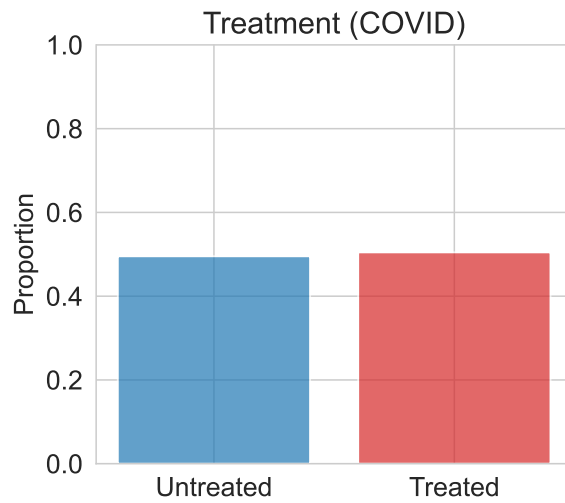


**Figure D.8:** Distribution of treatment status for the COVID-19 study. Proportion of Italian provinces classified as “Treated” (poorer distributed primary health care, defined as being above the national median for the ratio of adults to family doctors,  $n = 54$ ) and “Untreated” (better distributed primary care,  $n = 53$ ).

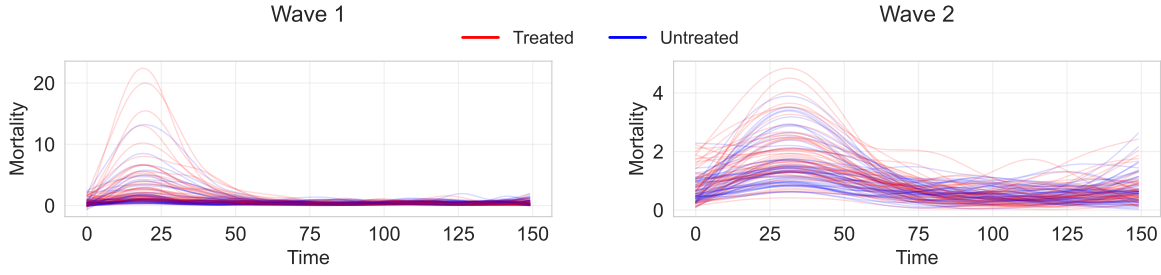


**Figure D.9:** Observed COVID-19 mortality functional outcome trajectories during the first and second waves.

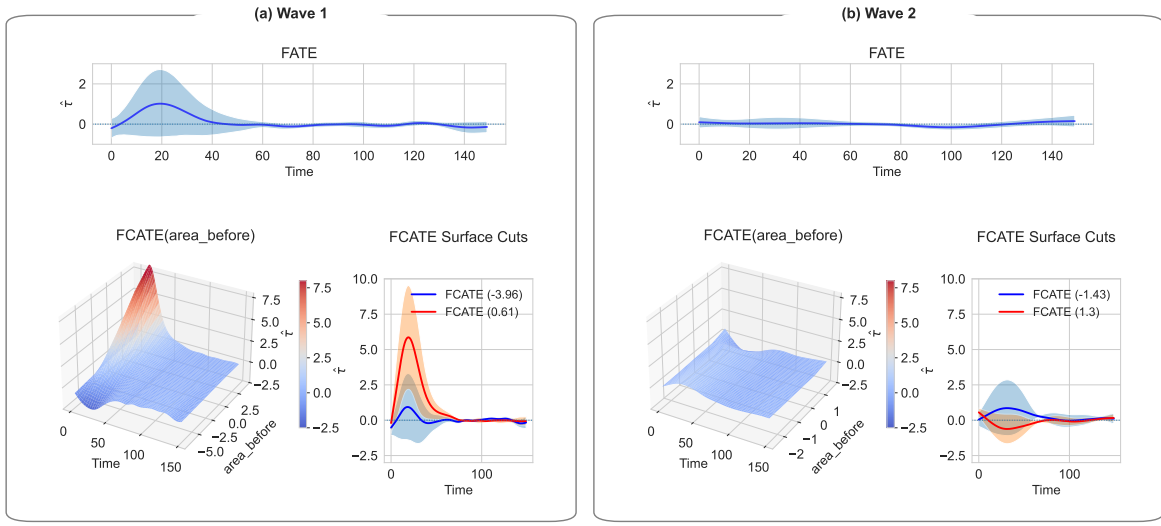


**Figure D.10:** Additional results on the heterogeneous impact of availability of primary health care on COVID-19 mortality patterns (COVID-19 study). Compared to Figure 4, here we set the conditioning variables to a higher quantile (0.6) as a robustness check.

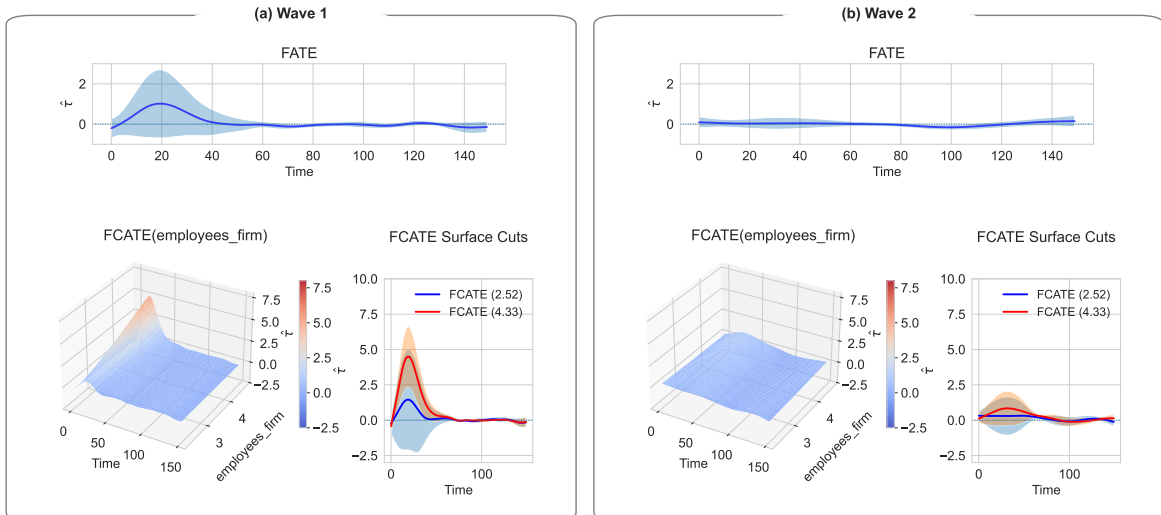


**Figure D.11:** F-CATE analysis of COVID-19 mortality conditioned on workplace. Panels can be interpreted as in Figure 4.